Copy No._____

Defence Research and Development Canada
Recherche et développement pour la défense Canada

DEFENCE R&D DÉFENSE

Simulation of Hydrodynamic Forces and Motions for a Freely Maneuvering Ship in a Seaway

Kevin McTaggart

Defence R&D Canada – Atlantic

Technical Memorandum
DRDC Atlantic TM 2005-071
December 2005

Canada

This page intentionally left blank.

Simulation of Hydrodynamic Forces and Motions for a Freely Maneuvering Ship in a Seaway

Kevin McTaggart

Defence R&D Canada – Atlantic
Technical Memorandum
DRDC Atlantic TM 2005-071
December 2005

Principal Author

Kevin McTaggart

Kevin McTaggart

Approved by

Neil Pegg

Neil Pegg
Head, Warship Performance

Approved for release by

K. Foster
Chair/Document Review Panel

Abstract

ShipMo3D is DRDC Atlantic's object-oriented library for modelling ship motions in waves. Previous ShipMo3D development considered ships travelling with nominally steady speed and heading. This report describes the extension of the ShipMo3D library to model motions of freely maneuvering ships. New ShipMo3D force components arise from hull maneuvering, resistance, propulsion, and rudder-propeller interaction. Comparisons of turning circle predictions with full-scale trials data for the tanker Esso Osaka give encouraging results. Comparisons of predictions with motions of a steered warship model in waves give very good results. Excellent agreement between predictions for a freely maneuvering ship and for a ship with nominally steady speed and heading indicates that the extension of ShipMo3D to freely maneuvering ships has been correctly implemented. It is recommended that future work further investigate prediction of hull maneuvering forces.

Résumé

ShipMo3D est la bibliothèque objet utilisée par RDDC Atlantique pour modéliser les mouvements des navires dans la houle. La version précédente de ShipMo3D se limitait aux navires se déplaçant avec une vitesse et un cap théoriquement constants. Dans ce rapport, nous décrivons les développements de la bibliothèque ShipMo3D visant la modélisation des mouvements des navires manœuvrant sans contraintes. Les nouvelles composantes de ShipMo3D simulent la force exercée sur la carène, la résistance, la propulsion et les interactions gouvernail-hélice. Les comparaisons des prédictions et des données tirées d'essais à échelle réelle de cercles de giration par le pétrolier Esso Osaka sont encourageantes, tout comme les comparaisons avec les mouvements d'une maquette dirigée de bâtiment de guerre. L'excellent accord entre les prédictions d'un navire manœuvrant sans contrainte et un navire navigant avec une vitesse et un cap théoriquement constants indique que les améliorations apportées à ShipMo3D visant les navires manœuvrant sans contraintes ont été correctement réalisées. Nous recommandons que les travaux à venir soient consacrés à une étude plus poussée de la prédiction des forces exercées sur la carène lors des manœuvres.

This page intentionally left blank.

Executive summary

Simulation of Hydrodynamic Forces and Motions for a Freely Maneuvering Ship in a Seaway

Kevin McTaggart; DRDC Atlantic TM 2005-071; Defence R&D Canada – Atlantic; December 2005.

Introduction: In support of DND work on modelling and simulation, DRDC Atlantic has developed the ShipMo3D library for simulation of ship motions in waves. Previous ShipMo3D development considered ships travelling with nominally steady speed and heading in waves. This report describes the extension of ShipMo3D to prediction of motions for freely maneuvering ships in calm water and in waves.

Principal Results: Forces relevant to ship maneuvering have been introduced to ShipMo3D. Comparisons of turning circles with full-scale trials data for the tanker Esso Osaka give encouraging results. Comparisons of predictions with motions of a steered warship model in waves give very good results. Excellent agreement between predictions for a freely maneuvering ship and for a ship with nominally steady speed and heading indicates that the extension of ShipMo3D to freely maneuvering ships has been correctly implemented.

Significance of Results: DND now has an object-oriented library for modelling of motions of freely maneuvering ships in calm water and in waves. This library can be used to develop applications in support of acquisition, operations, and training. For simulation of motions of existing ships, agreement between predicted and observed motions can be optimized by tuning of hull maneuvering force coefficients.

Future Plans: ShipMo3D applications and corresponding documentation will be developed to facilitate simulation of maneuvering ships in waves using input ASCII files. Documentation will also be developed for using ShipMo3D objects within simulations. Future work will also likely examine improved prediction of hull maneuvering coefficients.

Sommaire

Simulation of Hydrodynamic Forces and Motions for a Freely Maneuvering Ship in a Seaway

Kevin McTaggart; DRDC Atlantic TM 2005-071; R & D pour la défense Canada – Atlantique; décembre 2005.

Introduction: En appui aux travaux de modélisation et de simulation du MDN, RDDC Atlantique a créé la bibliothèque objet ShipMo3D consacrée à la simulation des mouvements des navires dans la houle. La version précédente de ShipMo3D se limitait aux navires se déplaçant avec une vitesse et un cap théoriquement constants par rapport à la houle. Dans ce rapport, nous décrivons les développements de la bibliothèque ShipMo3D visant la prédiction de mouvements des navires manœuvrant sans contraintes, sur une mer calme ou houleuse.

Résultats principaux: Les nouvelles composantes de ShipMo3D traitent les forces pertinentes à la manœuvre des navires. Les comparaisons des prédictions et des données tirées d'essais à échelle réelle de cercles de giration par le pétrolier Esso Osaka sont encourageantes, tout comme les comparaisons avec les mouvements d'une maquette dirigée de bâtiment de guerre. L'excellent accord entre les prédictions d'un navire manœuvrant sans contrainte et un navire navigant avec une vitesse et un cap théoriquement constants indique que les améliorations apportées à ShipMo3D visant les navires manœuvrant sans contraintes ont été correctement réalisées.

Importance des résultats: Le MDN dispose maintenant d'une bibliothèque objet pour la modélisation des navires manœuvrant sans contraintes sur une mer calme ou houleuse. On pourra utiliser cette bibliothèque pour élaborer des logiciels en appui à l'acquisition, aux opérations et à la formation. Lors de la simulation des mouvements de navires réels, on optimisera l'accord entre les mouvements prédits et observés, en ajustant les coefficients des forces exercées sur la carène lors des manœuvres.

Travaux ultérieurs prévus: Les applications de ShipMo3D et la documentation correspondante seront élaborées afin de faciliter la simulation de navires manœuvrant dans la houle, en utilisant des fichiers d'entrée en ASCII. On rédigera également la documentation relative à l'utilisation d'objets de la bibliothèque ShipMo3D lors des simulations.

Table of contents

List of tables

List of figures

1 Introduction

Naval modelling and simulation applications frequently require predictions of ship motions in calm water and in waves. DRDC Atlantic's ShipMo3D is an object oriented library being developed to meet requirements of a variety of simulation applications. Previous ShipMo3D developments [1, 2, 3, 4] consider the forces and resulting motions in waves for a ship travelling with nominally steady speed and heading.

The present work extends the ShipMo3D library to simulate the motions of a freely maneuvering ship in waves. Force components arising from hull lift, hull resistance, hull cross-flow drag, rudder lift and drag, and propeller thrust are important for a freely maneuvering ship and are incorporated into ShipMo3D. Unlike many ship maneuvering programs, the ShipMo3D library includes retardation forces essential for accurate modelling of ship motions in waves.

The next section gives a brief literature review of ship maneuvering prediction. Section 3 gives the axis systems and equations of motions for a freely maneuvering ship, followed by discussion of hull maneuvering forces in Section 4. Section 5 describes hull cross-flow drag forces and their relationship to the hull maneuvering forces in the previous section. Hull resistance and propulsion are described in Sections 6 and 7 respectively. Section 8 discusses rudder deflection forces, and is followed by treatment of rudder-propeller interaction forces in Section 9. Section 10 describes modelling of rudder and propeller control systems. Section 11 gives validation of turning circle predictions with full-scale trials data for the tanker Esso Osaka. Modelling of maneuvering using unclassified data for the Canadian Navy's HALIFAX class is described in Section 12. Section 13 gives validation for predicted motions in waves using experimental data for a steered warship model. Recommendations for future work are given in Section 14, followed by final conclusions in Section 15.

2 Literature Review of Ship Maneuvering Force Prediction

Ship maneuvering, also spelt "manoeuvring" and "maneuvring", has been the subject of extensive literature. For application within ShipMo3D, maneuvering simulation approaches of greatest interest are those which predict ship maneuvering properties based on hydrodynamic forces acting on the hull and appendages (including propeller), and aerodynamic forces acting on the superstructure. The present report only considers hydrodynamic forces. Incorporation of aerodynamic forces into ShipMo3D will likely be the subject of future work.

Several references provide good overviews of ship maneuvering forces. Bertram [5]

presents one of the most recent comprehensive discussions of maneuvering forces. His book also covers other relevant areas of ship hydrodynamics, including resistance, propulsion, and seakeeping. The International Towing Tank Conference Specialist Committee on Esso Osaka [6] have also produced a good recent reference on ship maneuvering forces, with emphasis on maneuvering predictions for the Esso Osaka, a tanker that has been the subject of extensive full-scale and model test studies. Barr [7] compares several different programs for simulating ship maneuvering. Burcher [8] discusses both model testing and mathematical approaches for predicting ship maneuvering forces. Crane et al. [9] give another general overview of ship maneuvering forces. Inoue et al. [10] present equations for estimating hull maneuvering forces based on model test data.

When considering the maneuvering literature in the context of ShipMo3D, it should be noted that ShipMo3D has been developed based primarily on the theory for ship seakeeping, which uses somewhat different definitions and approaches from those in the ship maneuvering field. The first major difference between the maneuvering and seakeeping approaches is that maneuvering predictions are usually based on ship-fixed axes, while seakeeping predictions are usually based on translating earth axes. The second major difference is that maneuvering predictions usually assume that hull forces are independent of frequency of motion, while seakeeping predictions duely consider the influence of motion frequency. Consequently, care must be taken when applying results from the maneuvering literature to ShipMo3D.

3 Axis Systems and Equations of Motion for ShipMo3D Computations

Previous ShipMo3D reports [1, 2, 3, 4] consider the motions in waves of a ship with quasi-steady speed and heading. This report introduces motions for a freely maneuvering ship, which must ultimately be expressed using earth-fixed axes. ShipMo3D's earth-fixed axis system is shown in Figure 1, and was first introduced in Reference 3. The instantaneous heading (to) of the ship is denoted χ and the heading (from) of ocean waves is denoted ν.

In keeping with ShipMo3D's seakeeping pedigree, the ship motions are solved using the translating earth coordinate system shown in Figure 2. When ocean waves are present, their direction relative to the ship is given according to Figure 3. For large amplitude motions, forces on the ship can be evaluated using the ship based axis system of Figure 4 and then transformed to translating earth axes.

When computing ship motions in the time domain, it is necessary to select a suitable nominal heading and nominal speed for orienting the translating earth coordinate sys-

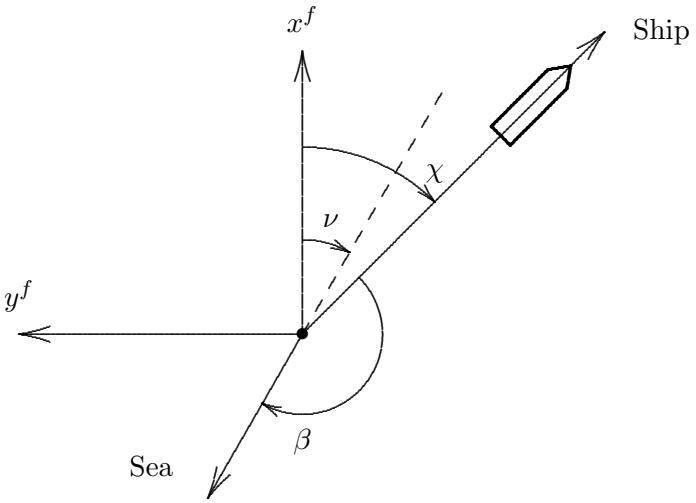

Figure 1: *Earth-Fixed Coordinate System*

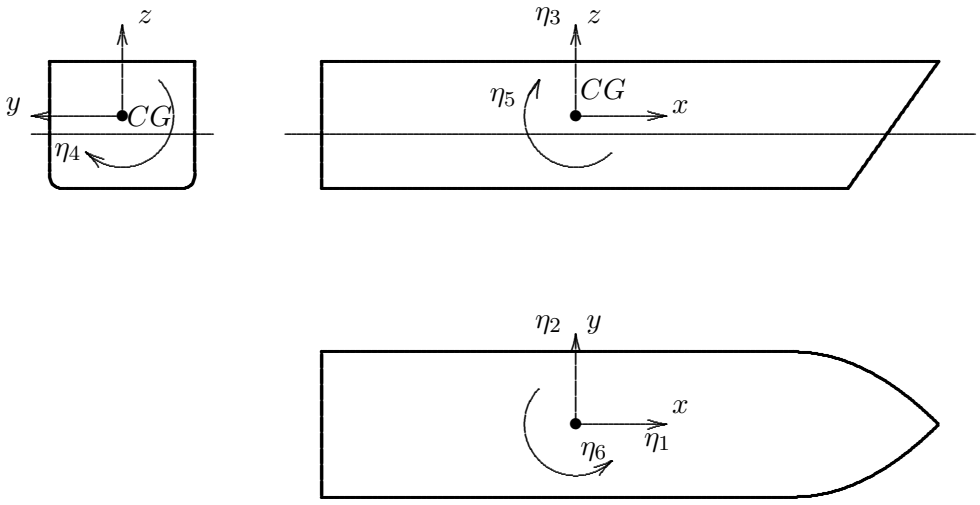

Figure 2: *Translating Earth Coordinate System*

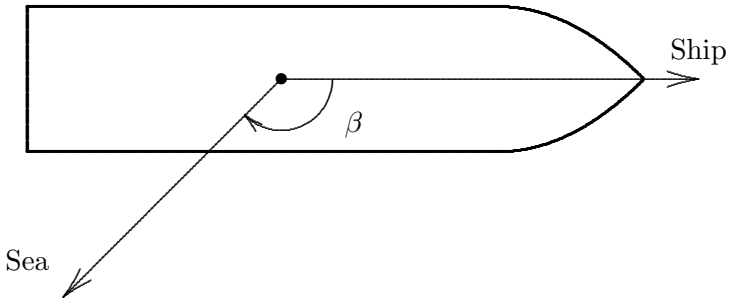

Figure 3: *Sea Direction Relative to Ship*

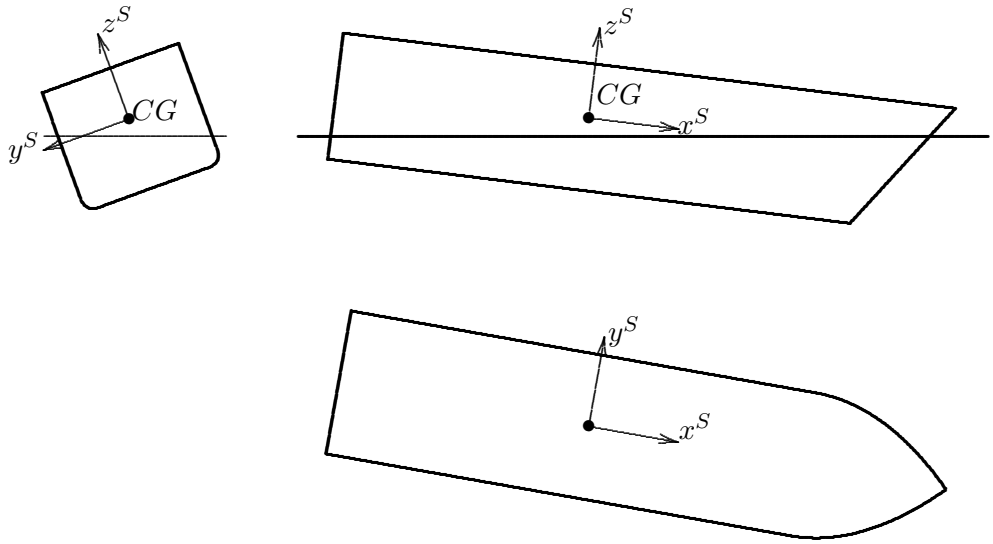

Figure 4: *Ship Referenced Coordinate System for Large Angular Motions*

tem used to solve the ship motions at each time step. Computations with ShipMo3D indicate that the translating earth coordinate system can be oriented based on the instantaneous heading and ship speed along that heading at each time step.

During each time step of a time domain simulation, the forces and resulting accelerations are computed in translating earth axes. The resulting accelerations in earth-fixed axes are:

$$\ddot{x}_f = \ddot{\eta}_1 \cos\chi - \ddot{\eta}_2 \sin\chi \quad (1)$$

$$\ddot{y}_f = -\ddot{\eta}_1 \sin\chi + \ddot{\eta}_2 \chi \quad (2)$$

$$\ddot{\chi} = -\ddot{\eta}_6 \quad (3)$$

Heave, roll, and pitch are equivalent in earth-fixed and translating axis systems.

The equations of motion in the time domain include terms presented in earlier reports [2, 4], and new terms introduced in this report that are important for a freely maneuvering ship. These new terms include forces due to resistance, propulsion, rudder-propeller interaction, hull maneuvering (which can include lift and viscous contributions), and hull cross-flow drag. The equations of motion are:

$$\begin{aligned}
([M] + [A(U,\infty)])\ \{\ddot{\eta}(t)\} &= \\
&- \left[B(U,\infty,\vec{\dot{\eta}})\right]\ \{\dot{\eta}(t)\} - \int_{-\infty}^{t} \left[K^{hull}(U,t-\tau)\right]\{\dot{\eta}(\tau)\}\ d\tau \\
&- \left[C(U,\infty,\vec{\eta})\right]\{\eta(t)\} + \left\{F^{I}(t)\right\} + \left\{F^{D}(t)\right\} + \{F^{cross}(t)\} \\
&+ \left\{F^{resist}(t)\right\} + \{F^{prop}(t)\} + \left\{F^{rudder-deflect}(t)\right\} \\
&+ \left\{F^{rudder-prop}(t)\right\} \quad (4)
\end{aligned}$$

The ship inertia matrix $[M]$ is based on the dry ship. The added mass matrix $[A(U,\infty)]$ is the infinite frequency value dependent on ship speed U, and includes contributions from the hull and appendages as follows:

$$\begin{aligned}
[A(U,\infty)] = \left[A^{hull}(U,\infty)\right] &+ \sum_{i=1}^{N_{foil}} \left[A^{foil-i}\right] + \sum_{i=1}^{N_{rudder}} \left[A^{rudder-i}\right] \\
&+ \sum_{i=1}^{N_{skeg}} \left[A^{skeg-i}\right] + \sum_{i=1}^{N_{bk}} \left[A^{bk-i}\right] \quad (5)
\end{aligned}$$

where $[A^{hull}]$ is the hull added mass, $[A^{foil-i}]$ is the added mass for static foil i (e.g., propeller shaft bracket), $[A^{rudder-i}]$ is the added mass for rudder i, $[A^{skeg-i}]$ is the added mass for skeg i, and $[A^{bk-i}]$ is the added mass for bilge keel i. The appendage added masses are independent of speed and frequency of motion. The damping matrix

includes contributions from the hull and appendages as follows:

$$\begin{aligned}\left[B(U,\infty,\vec{\eta})\right] &= \left[b^{hull-rad}(U)\right] + \left[B^{hull-man}(U,\vec{\eta})\right] \\ &+ \left[B^{hull-visc}(U,|\dot{\eta}_4|)\right] + \sum_{i=1}^{N_{foil}} \left[B^{foil-i}(U,|\dot{\eta}_4|)\right] \\ &+ \sum_{i=1}^{N_{rudder}} \left[B^{rudder-i}(U,|\dot{\eta}_4|)\right] + \sum_{i=1}^{N_{skeg}} \left[B^{skeg-i}(U,|\dot{\eta}_4|)\right] \\ &+ \sum_{i=1}^{N_{bk}} \left[B^{bk-i}(U,|\dot{\eta}_4|)\right] \end{aligned} \tag{6}$$

where $[b^{hull-rad}]$ is the hull frequency independent damping due to the potential flow, $[B^{hull-man}]$ is the hull maneuvering damping, which can include forces from lift and cross-flow drag, $[B^{hull-visc}]$ is the hull viscous damping due to roll, $[B^{foil-i}]$ is the damping for static foil i, $[B^{rudder-i}]$ is the damping for rudder i, $[B^{skeg-i}]$ is the damping for skeg i, and $[B^{bk-i}]$ is the damping for bilge keel i. The retardation function matrix $[K^{hull}]$ is due to the dependence of hull hydrodynamic forces on frequency of motion. The stiffness matrix includes contributions from buoyancy, hull potential flow forces, and hull and appendage lift forces as follows:

$$\begin{aligned}\left[C(U,\infty,\vec{\eta})\right] &= \left[C^{buoy}\right] + \left[c^{hull}(U)\right] + \left[C^{hull-man}(U,\vec{\eta})\right] \\ &+ \sum_{i=1}^{N_{foil}} \left[C^{foil-i}(U)\right] + \sum_{i=1}^{N_{rudder}} \left[C^{rudder-i}(U)\right] \\ &+ \sum_{i=1}^{N_{skeg}} \left[C^{skeg-i}(U)\right] + \sum_{i=1}^{N_{bk}} \left[C^{bk-i}(U)\right] \end{aligned} \tag{7}$$

where $[C^{buoy}]$ is the hull buoyancy stiffness, $[c^{hull}]$ is the hull frequency independent stiffness due to the potential flow, $[C^{hull-man}]$ is the hull stiffness due to maneuvering forces, $[C^{foil-i}]$ is the lift stiffness for static foil i, $[C^{rudder-i}]$ is the lift stiffness for rudder i, $[C^{skeg-i}]$ is the lift stiffness for skeg i, and $[C^{bk-i}]$ is the lift stiffness for bilge keel i. The incident wave excitation vector $\{F^I\}$ consists of the following:

$$\begin{aligned}\left\{F^I(t)\right\} &= \left\{F^{I-hull}(t)\right\} + \sum_{i=1}^{N_{foil}} \left\{F^{I-foil-i}(t)\right\} + \sum_{i=1}^{N_{rudder}} \left\{F^{I-rudder-i}(t)\right\} \\ &+ \sum_{i=1}^{N_{skeg}} \left\{F^{I-skeg-i}(t)\right\} + \sum_{i=1}^{N_{bk}} \left\{F^{I-bk-i}(t)\right\} \end{aligned} \tag{8}$$

where $\{F^{I-hull}\}$ is the incident wave force on the hull, $\{F^{I-foil-i}\}$ is the incident wave force on foil i, $\{F^{I-rudder-i}\}$ is the incident wave force on rudder i, $\{F^{I-skeg-i}\}$

is the incident wave force on skeg i, and $\{F^{I-bk-i}\}$ is the incident wave force on bilge keel i. The wave diffraction force vector $\{F^D\}$ typically only consists of hull forces, unless panelled appendages are included in diffraction computations [4].

The hull cross-flow drag $\{F^{cross}\}$, ship resistance $\{F^{resist}\}$, propulsion $\{F^{prop}\}$, rudder deflection $\{F^{rudder-deflect}\}$, and rudder-propeller interaction $\{F^{rudder-prop}\}$ are important force components for a freely maneuvering ship, and are discussed in Sections 5 to 9.

Some ship force components are most easily computed using ship-fixed axes, followed by translation to translating earth axes. Figure 4 shows ship-based axes, which can vary significantly from translating earth axes when motion amplitudes are large. Within ShipMo3D, ship resistance and propulsion forces are assumed to act along the x^S direction of ship-based axes. If buoyancy and incident wave forces are computed using integration of panel pressures in the time domain, then these components are also evaluated using ship-fixed axes.

After selected force components are computed in ship-based axes, they are transformed to translating earth axes using the following:

$$\begin{aligned}
F_1(t) &= F_1^S(t)\ \cos\eta_5\ \cos\eta_6 \\
&\quad - F_2^S(t)\ (-\cos\eta_4\ \sin\ \eta_6\ +\ \sin\eta_4\ \sin\eta_5\ \cos\eta_6) \\
&\quad + F_3^S(t)\ (\cos\eta_4\ \sin\eta_5\ \cos\eta_6\ +\ \sin\eta_4\ \sin\eta_6) && (9) \\
F_2(t) &= F_1^S(t)\ \cos\eta_5\ \sin\eta_6 \\
&\quad + F_2^S(t)\ (\cos\eta_4\ \cos\eta_6\ +\ \sin\eta_4\ \sin\eta_5\ \sin\eta_6) \\
&\quad + F_3^S(t)\ (\cos\eta_4\ \sin\eta_5\ \sin\eta_6\ -\ \sin\eta_4\ \cos\eta_6) && (10) \\
F_3(t) &= -F_1^S(t)\ \sin\eta_5\ +\ F_2^S(t)\ \sin\eta_4\ \cos\eta_5 \\
&\quad + F_3^S(t)\ \cos\eta_4\ \cos\eta_5 && (11) \\
F_4(t) &= F_4^S(t) && (12) \\
F_5(t) &= F_5^S(t)\ \cos\eta_4\ -\ F_6^S(t)\sin\eta_4 && (13) \\
F_6(t) &= F_5^S(t)\ \sin\eta_4\ +\ F_6^S(t)\cos\eta_4 && (14)
\end{aligned}$$

where F_j is the force for mode j in translating earth axes, and F_j^S is the force for mode j in ship-based earth axes.

For a ship executing a turning circle, several terms are used to describe the turning circle characteristics, as illustrated in Figure 5. Dimensions are typically referenced to the point at which rudder deflection was initiated. The advance refers to the displacement in the direction of the initial heading, and the transfer refers to the displacement lateral to the the direction of the initial heading. The terms advance and transfer are both often applied to either any point on a turning circle or to the specific point at which the ship heading has changed by 90 degrees relative to the

original heading. The tactical diameter is the transfer when the heading has changed by 180 degrees.

4 Hull Maneuvering Forces

To provide accurate maneuvering predictions, ShipMo3D requires new hull maneuvering force terms that have not been previously included for ShipMo3D seakeeping calculations. These new hull force terms are due primarily to forces arising from lift on the hull and cross-flow drag. The hull maneuvering force terms are expressed within ShipMo3D such that they can be determined from standard maneuvering test results if available.

The prediction of hull maneuvering forces is discussed in many references. ShipMo3D estimates hull maneuvering forces based on Inoue et al. [10], who developed equations based on physical considerations and analysis of model test data. Sway and yaw damping coefficients include both linear and nonlinear terms, and are expressed as:

$$B_{22}^{hull-man} = U\ B_{22U}^{hull-man} + U\ |v'|\ B_{22U|v'|}^{hull-man} + U\ |r'|\ B_{22U|r'|}^{hull-man} \quad (15)$$

$$B_{26}^{hull-man} = U\ B_{26U}^{hull-man} + U\ |r'|\ B_{26U|r'|}^{hull-man} \quad (16)$$

$$B_{62}^{hull-man} = U\ B_{62U}^{hull-man} + U\ r'^2\ B_{62Ur'^2}^{hull-man} \quad (17)$$

$$B_{66}^{hull-man} = U\ B_{66U}^{hull-man} + U\ |r'|\ B_{66U|r'|}^{hull-man} + U\ v'^2\ B_{66Uv'^2}^{hull-man} \quad (18)$$

The non-dimensional sway velocity v' is given by:

$$v' = \frac{\dot{\eta}_2}{U} \quad (19)$$

The non-dimensional yaw rate is given by:

$$r' = \frac{\dot{\eta}_6\ L}{U} \quad (20)$$

Inoue et al. present methods for computing the relevant terms in Equations (15) to (18). When computing linear terms for the above equations, it must be noted that equations in Inoue et al. include contributions due to hull radiation forces, which are already included in the ShipMo3D library. The resulting hull maneuvering terms computed using nondimensional coefficients based on Inoue et al. are:

$$B_{22U}^{hull-man} = -\frac{1}{2}\ \rho\ L\ T_{mid}\ Y_v' - B_{22U}^{hull-rad}(\omega_e = \infty) \quad (21)$$

$$B_{26}^{hull-man} = -\frac{1}{2}\ \rho\ L^2\ T_{mid}\ Y_r' - B_{26U}^{hull-rad}(\omega_e = \infty) \quad (22)$$

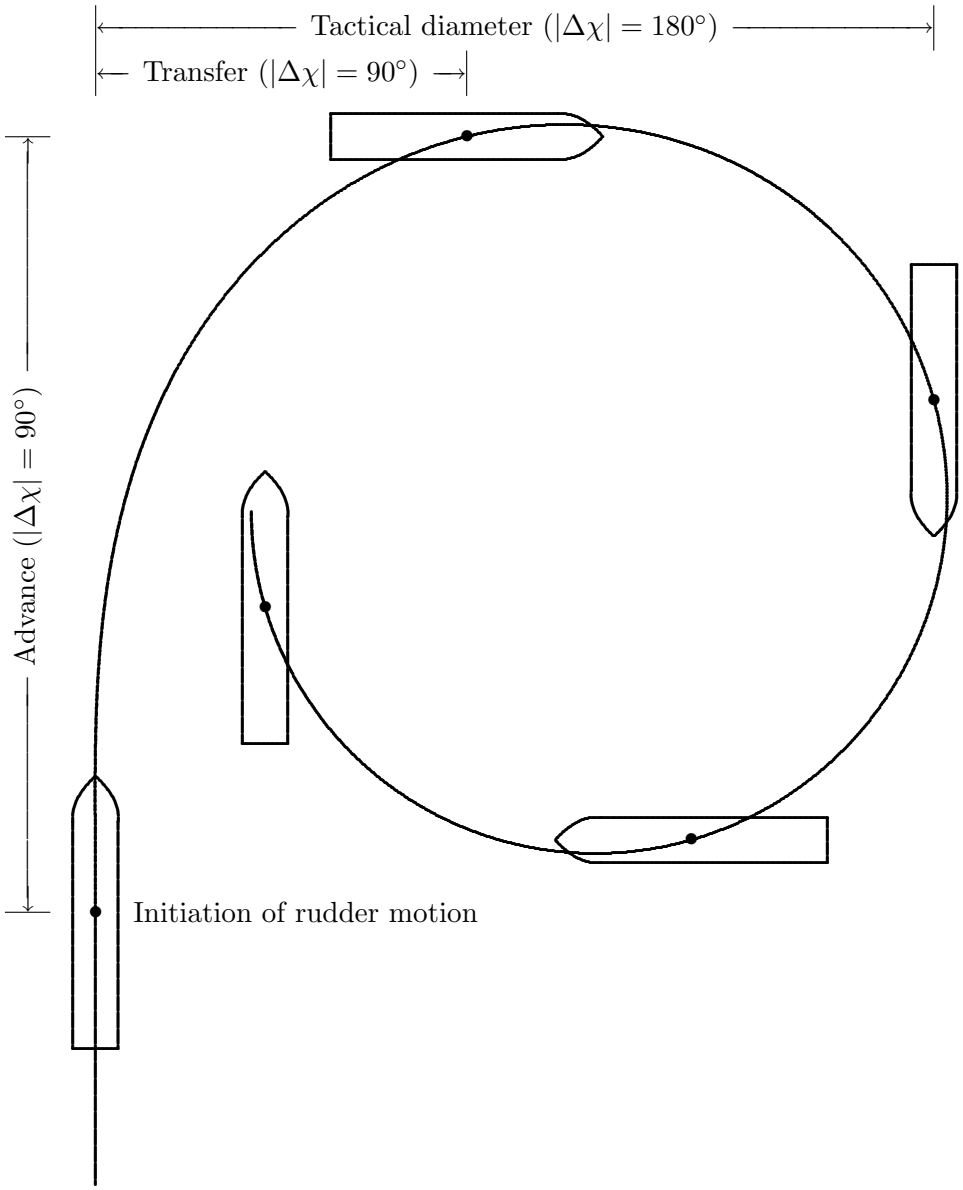

Figure 5: *Turning Circle Characteristics*

$$B_{62}^{hull-man} = -\frac{1}{2}\,\rho\,L^2\,T_{mid}\,N'_v - B_{62U}^{hull-rad}(\omega_e=\infty) \quad (23)$$

$$B_{66}^{hull-man} = -\frac{1}{2}\,\rho\,L^3\,T_{mid}\,N'_r - B_{66U}^{hull-rad}(\omega_e=\infty) \quad (24)$$

where T_{mid} is draft at midships. The hull radiation damping terms to be subtracted from the above equations are given in Reference 2 as follows:

$$B_{j2U}^{hull-rad}(\omega_e=\infty) = -\frac{\widetilde{\partial A}_{j2}^{hull}(U=0,\omega_e=\infty)}{\partial x} \quad (25)$$

$$B_{j6U}^{hull-rad}(\omega_e=\infty) = -A_{j2}^{hull}(U=0,\omega_e=\infty) - \frac{\widetilde{\partial A}_{j6}^{hull}(U=0,\omega_e=\infty)}{\partial x} \quad (26)$$

where $\widetilde{\partial A}_{jk}^{hull}/\partial x$ is determined from the x derivative of potentials giving added mass and A_{j2}^{hull} is added mass due to sway motion, with $U=0$ denoting zero forward speed and $\omega_e=\infty$ denoting infinite encounter frequency.

The linear nondimensional coefficients for hull maneuvering forces are obtained based on Inoue et al., with sign changes to conform to conventions commonly used within the maneuvering literature:

$$Y'_v = -\left(\pi\,\frac{T_{mid}}{L} + 1.4\,C_B\,\frac{B}{L}\right)\left(1 + \frac{2\,t_{stern}}{3\,T_{mid}}\right) \quad (27)$$

$$Y'_r = \frac{\pi}{2}\,\frac{T_{mid}}{L}\left(1 + 0.8\frac{t_{stern}}{T_{mid}}\right) \quad (28)$$

$$N'_v = -\frac{2T_{mid}}{L}\left(1 - \frac{0.27}{l_\alpha}\,\frac{t_{stern}}{T_{mid}}\right) \quad (29)$$

$$N'_r = -\left[0.54\,\frac{2\,T_{mid}}{L} - \left(\frac{2T_{mid}}{L}\right)^2\right]\left(1 + 0.30\,\frac{t_{stern}}{T_{mid}}\right) \quad (30)$$

where C_B is block coefficient, B is beam, and t_{stern} is trim by stern. The term l_β in Equation (29) is given by:

$$l_\beta = \frac{2\,T_{mid}}{\pi\,T_{mid} + 1.4\,C_B\,B} \quad (31)$$

The nonlinear hull maneuvering force terms are given by:

$$B_{22U|v'|}^{hull-man} = -\frac{1}{2}\,\rho\,L\,T_{mid}\,Y'_{v|v|} \quad (32)$$

$$B_{22U|r'|}^{hull-man} = -\frac{1}{2}\,\rho\,L\,T_{mid}\,Y'_{v|r|} \quad (33)$$

$$B_{26U|r'|}^{hull-man} = -\frac{1}{2}\,\rho\,L^2\,T_{mid}\,Y'_{r|r|} \tag{34}$$

$$B_{62Ur'^2}^{hull-man} = -\frac{1}{2}\,\rho\,L^2\,T_{mid}\,N'_{vr^2} \tag{35}$$

$$B_{66U|r'|}^{hull-man} = -\frac{1}{2}\,\rho\,L^3\,T_{mid}\,N'_{r|r|} \tag{36}$$

$$B_{66Uv'^2}^{hull-man} = -\frac{1}{2}\,\rho\,L^3\,T_{mid}\,N'_{rv^2} \tag{37}$$

The non-dimensional terms in the above equations are evaluated based on Inoue et al., with signs changed to conform to conventions commonly used in the maneuvering literature:

$$Y'_{v|v|} = 0.09 - 6.5\,(1 - C_B)\,\frac{T_{mid}}{B} \tag{38}$$

$$Y'_{v|r|} = -0.44 + 1.78\,(1 - C_B)\,\frac{T_{mid}}{B} \tag{39}$$

$$Y'_{r|r|} = 0.0 \tag{40}$$

$$N'_{vr^2} = 0.0 \tag{41}$$

$$N'_{r|r|} = \begin{cases} -0.060 & \text{for } \frac{C_B B}{L} < 0.06 \\ -0.146 + 1.8\frac{C_B B}{L} - 6\left(\frac{C_B B}{L}\right)^2 & \text{for } 0.06 \le \frac{C_B B}{L} \le 0.2 \\ -0.026 & \text{for } \frac{C_B B}{L} > 0.2 \end{cases} \tag{42}$$

$$N'_{r'v^2} = -0.2 \tag{43}$$

The terms $Y'_{r|r|}$ and N'_{vr^2} in the above equations are set to zero because of the significant scatter in measured values.

Experimental data presented by Inoue et al. suggest that actual nondimensional maneuvering coefficients can vary significantly from those predicted using Equations (27) to (30) and (38) to (43). Table 1 gives nominal uncertainties associated with estimated hull force coefficients. The uncertainties in Table 1 have been set such that actual maneuvering coefficients are likely to fall within the specified range.

The maneuvering forces presented thus far consider only sway and yaw. In the current work, the vertical location of the lateral hull maneuvering force is assumed to act at the waterline based on Bertram [5]. The location of the hull maneuvering force relative to the centre of gravity is given by:

$$\overline{z}^{hull-man} = -\,z_{wl}^{CG} \tag{44}$$

where z_{wl}^{CG} is the location of the ship centre of gravity relative to the calm waterline. The above vertical location is also assumed to be the reference point for lateral motions influencing hull maneuvering forces. The following terms can then be derived:

$$B_{24}^{hull-man} = -B_{22}^{hull-man}\,\overline{z}^{hull-man} \tag{45}$$

$$B_{42}^{hull-man} = -B_{22}^{hull-man}\ \overline{z}^{hull-man} \quad (46)$$

$$B_{44}^{hull-man} = B_{22}^{hull-man}\ \left(\overline{z}^{hull-man}\right)^2 \quad (47)$$

$$B_{46}^{hull-man} = -B_{26}^{hull-man}\ \overline{z}^{hull-man} \quad (48)$$

$$B_{64}^{hull-man} = -B_{62}^{hull-man}\ \overline{z}^{hull-man} \quad (49)$$

It should be noted that the approach developed by Inoue et al. for predicting hull maneuvering coefficients is intended for hulls with lateral profiles approximating a rectangle. For ships such as frigates having significant variation of draft with longitudinal location, care should be taken in applying the method of Inoue et al. for predicting hydrodynamic coefficients.

Table 1: *Uncertainties for Estimated Nondimensional Hull Maneuvering Coefficients*

Y'_v	± 0.05
Y'_r	± 0.05
N'_v	± 0.02
N'_r	± 0.02
$Y'_{v\|v\|}$	± 0.2
$Y'_{v\|r\|}$	± 0.2
$Y'_{r\|r\|}$	± 0.05
N'_{vr^2}	± 0.05
$N'_{r\|r\|}$	± 0.02
N'_{rv^2}	± 0.2

5 Separate Treatment of Hull Cross-Flow Drag Forces

The hull maneuvering force terms presented in the previous section typically include the effects of cross-flow drag. Alternatively, it is possible evaluate hull cross-flow drag separately, as discussed by Bertram [5]. For a ship exposed to a uniform cross-flow velocity of v^{cross}, the cross-flow drag force will be:

$$F^{cross} = \frac{1}{2}\,\rho\, v^{cross}\ |v^{cross}|\ A_y\, C_{Dy} \quad (50)$$

where A_y is the hull lateral profile area. The hull cross-flow drag velocity acting on a maneuvering ship is caused by the sway and yaw motion of the ship, and varies along

the ship hull. If cross-flow drag is computed separately from other hull maneuvering forces within ShipMo3D, then the hull is divided into a number of longitudinal segments (typically 10-20) for evaluation of the cross-flow drag as follows:

$$F_2^{cross} = \frac{1}{2}\,\rho\,\sum_{i=1}^{N_{seg}} v^{cross}(\overline{x}_{Ay-i})\;\left|v^{cross}(\overline{x}_{Ay-i})\right|\;A_{y-i}\,C_{Dy} \tag{51}$$

where N_{seg} is the number of hull longitudinal sections, $\overline{x}_{Ay-i}$ is the nominal x coordinate of section i, A_{y-i} is the lateral profile area of section i, and C_{Dy} is the cross-flow drag coefficient. The local hull cross-flow velocity is given by:

$$v^{cross}(\overline{x}_{Ay-i}) = -\dot{\eta}_2 - \overline{x}_{Ay-i}\,\dot{\eta}_6 \tag{52}$$

The roll and yaw cross-flow drag forces are evaluated in a manner similar to the sway cross-flow drag force:

$$F_4^{cross} = -\frac{1}{2}\,\rho\,\sum_{i=1}^{N_{seg}} v^{cross}(\overline{x}_{Ay-i})\;\left|v^{cross}(\overline{x}_{Ay-i})\right|\;A_{y-i}\,\overline{z}_{Ay-i}\,C_{Dy} \tag{53}$$

$$F_6^{cross} = \frac{1}{2}\,\rho\,\sum_{i=1}^{N_{seg}} v^{cross}(\overline{x}_{Ay-i})\;\left|v^{cross}(\overline{x}_{Ay-i})\right|\;A_{y-i}\,\overline{x}_{Ay-i}\,C_{Dy} \tag{54}$$

where $\overline{z}_{Ay-i}$ is the nominal z coordinate of the underwater profile for hull longitudinal segment i. The geometric properties of the hull longitudinal segments are evaluated based on the wet panelled hull surface using the following:

$$A_{y-i} = \frac{1}{2}\,\sum_{j=1}^{N_{p-i}} A_k(i,j)\;\left|n_{y-k(i,j)}\right| \tag{55}$$

$$\overline{x}_{Ay-i} = \frac{1}{2A_{y-i}}\,\sum_{j=1}^{N_{p-i}} A_k(i,j)\;\left|n_{y-k(i,j)}\right|\;\overline{x}_{k(i,j)} \tag{56}$$

$$\overline{z}_{Ay-i} = \frac{1}{2A_{y-i}}\,\sum_{j=1}^{N_{p-i}} A_{k(i,j)}\;\left|n_{y-k(i,j)}\right|\;\overline{z}_k(i,j) \tag{57}$$

where N_{p-i} is the number of hull panels whose centroid lies within hull longitudinal segment i, $k(i,j)$ is the global hull panel index for panel j on longitudinal segment i, A_k is the area of hull panel k, n_{y-k} is the y normal component for hull panel k, $\overline{x}_k$ is the x coordinate of the centroid of hull panel k, and $\overline{z}_k$ is the z coordinate of the centroid of hull panel k.

Bertram presents lateral drag coefficients ranging from 0.56 to 0.98 for four different ships. It is expected that lateral drag coefficients for most ships will be between 0.5 and 1.1.

As previously noted, hull cross-flow drag forces are typically included in hull maneuvering force coefficients. When including cross-flow drag in maneuvering coefficients, there appears to be an implicit assumption that the cross-flow velocity is small relative to ship forward velocity. In some cases, such as towing operations, the cross-flow velocity can be a significant fraction of the ship forward velocity. In such cases, it is likely more appropriate to model cross-flow drag forces separately from other hull maneuvering forces.

6 Hull Resistance Forces

Several references provide good overviews on hull resistance forces, including Bertram [5], Newman [11], and van Manen and van Oossanen [12]. ShipMo3D evaluates hull resistance forces using input resistance coefficients which are given as a function of ship speed:

$$F_1^{resist} = -\frac{1}{2}\,\rho\,U\,|U|\,A_w\,C_{Dx}(U) \tag{58}$$

where A_w is the hull wetted surface area and C_{Dx} is the ship resistance coefficient. Experimental data and CFD computations are among the available methods for selecting suitable resistance coefficient values.

7 Propeller Forces

Modelling of propeller forces is covered in many references, including Holtrop and Mennen [13, 14], Holtrop [15], and Van Manen and Van Oossanen [16]. The thrust created by the propeller can be expressed by:

$$F^{prop} = (1 - t_{prop})\,\rho\,n_{prop}^2\,D_{prop}^4\,K_T(J_{prop}) \tag{59}$$

where t_{prop} is the propeller thrust deduction coefficient, n_{prop} is the propeller speed in revolutions per second, and D_{prop} is the propeller diameter. The propeller thrust coefficient K_T is a function of the advance coefficient J_{prop}, which is given by:

$$J_{prop} = \frac{U\,(1 - w_{prop})}{n_{prop}\,D_{prop}} \tag{60}$$

where w_{prop} is the propeller wake fraction. Both the thrust deduction coefficient t_{prop} and propeller wake fraction w_{prop} tend to increase with hull block coefficient, and are generally larger for single screw ships than for twin-screw ships. Thrust deduction coefficients typically fall within the range $0.0 \leq t_{prop} \leq 0.2$, and propeller wake fractions typically fall within the range $0.0 \leq w_{prop} \leq 0.4$.

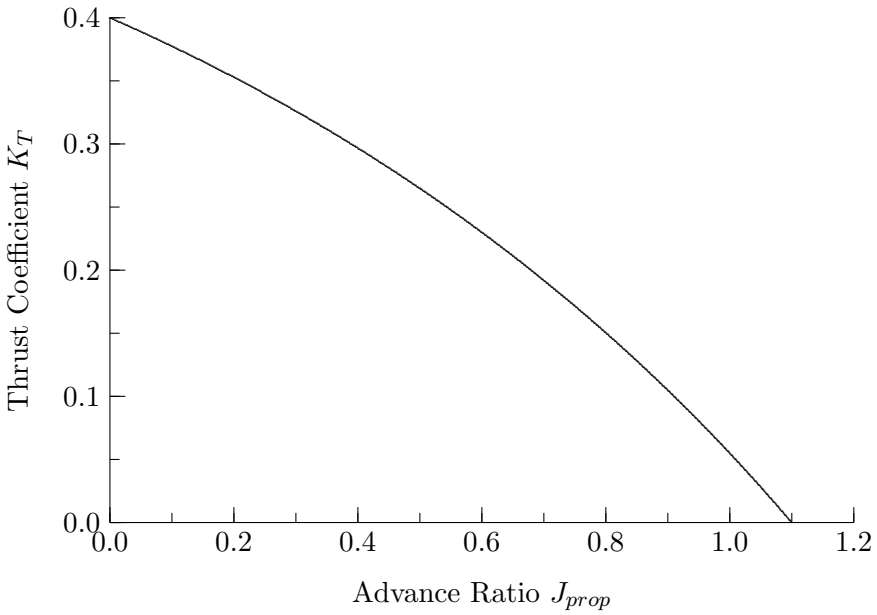

Figure 6: *Example Curve of Propeller Thrust Coefficient K_T Versus Advance Coefficient J_{prop} (adapted from Reference 16)*

The propeller thrust coefficient K_T decreases with increasing advance coefficient J_{prop}. Figure 6 shows an example thrust coefficient curve adapted from Reference 16.

ShipMo3D assumes that the propeller thrust acts along the ship longitudinal axis. Transformation to force components in translating earth axes is done using Equations (9), (10) and (11).

8 Rudder Deflection Forces

Forces arising from deflection of rudders (and other deflectable appendages) are computed as follows:

$$\begin{aligned}\left\{F^{rudder-deflect}(t)\right\} &= -\sum_{i=1}^{N_{rudder}} \left[C_{\eta\delta}^{rudder-i}(U)\right]\ \delta^{rudder-i} \\ &\quad + \sum_{i=1}^{N_{rudder}} \left\{F^{rudder-drag-i}\right\} \end{aligned} \tag{61}$$

where $[C_{\eta\delta}^{rudder-i}]$ is the stiffness matrix for ship forces arising from rudder deflections for rudder i, $\delta^{rudder-i}$ is the deflection of rudder i, and $\{F^{rudder-drag-i}\}$ is the drag forces vector on rudder i. ShipMo3D uses a rudder deflection convention of positive for counter-clockwise rotation when viewed from inside the ship. The rudder deflection stiffness terms are evaluated based on Reference 4. ShipMo3D calculations for rudder drag forces are based on Inoue et al. [17] as follows:

$$F_1^{rudder-deflect} = -F_N^{rudder}\ \sin\delta^{rudder} \tag{62}$$

where F_N^{rudder} is the total force normal to the rudder, including contributions from ship motions in waves. The force normal to the rudder is evaluated as follows:

$$F_2^{rudder} = -\sum_{j=1}^{6} B_{2j}^{rudder}\ \dot{\eta}_j - \sum_{j=1}^{6} C_{2j}^{rudder}\ \eta_j - \sum_{j=1}^{6} C_{2\delta}^{rudder}\ \delta^{rudder} \tag{63}$$

$$F_3^{rudder} = -\sum_{j=1}^{6} B_{3j}^{rudder}\ \dot{\eta}_j - \sum_{j=1}^{6} C_{3j}^{rudder}\ \eta_j - \sum_{j=1}^{6} C_{3\delta}^{rudder}\ \delta^{rudder} \tag{64}$$

$$F_N^{rudder} = F_2^{rudder}\ \cos\Gamma_{rudder} - F_3^{rudder}\ \sin\Gamma_{rudder} \tag{65}$$

where F_2^{rudder} is the total rudder lateral force, B_{ij}^{rudder} is rudder force damping due to ship motion mode j, C_{ij}^{rudder} is rudder force stiffness due to ship motion mode j, $C_{i\delta}^{rudder}$ is rudder force stiffness due to rudder deflection, F_3^{rudder} is total rudder vertical force, and Γ_{rudder} is rudder dihedral angle (0°for rudder to port, 90°for rudder upward).

9 Rudder-Propeller Interaction Forces

The rudder forces presented in Reference 4 and in the previous section do not consider the influence of propellers. To increase the steering efficiency of rudders, they are typically placed within the slipstream of ship propellers. The resulting rudder forces are significantly greater than if the rudder were placed outside of the propeller

slipstream. ShipMo3D models the influence of the propeller on rudder forces using an approach developed by Söding [18]. In addition to the rudder lift proportional to U^2 presented in Reference 4, the presence of the propeller induces the following lift and drag on a rudder in the propeller slipstream:

$$F_{lift}^{rudder-prop} = C^{rudder-prop}\ F^{prop}\ \left(1 + \frac{1}{\sqrt{1+C_{th}}}\right)\ \sin\delta^{rudder} \tag{66}$$

$$F_{drag}^{rudder-prop} = -C^{rudder-prop}\ F^{prop}\ \left(1 + \frac{1}{\sqrt{1+C_{th}}}\right)\ \left(1\ -\ \cos\delta^{rudder}\right) \tag{67}$$

where $C^{rudder-prop}$ is a rudder-propeller interaction coefficient, and C_{th} is the thrust loading coefficient of the propeller. The rudder-propeller interaction coefficient normally ranges between 0.0 and 1.0, increasing with proximity of the rudder to the propeller and with size of the rudder relative to the propeller. The effect of increasing rudder size becomes negligible when the rudder span exceeds twice the propeller diameter. The propeller thrust loading coefficient C_{th} is given by:

$$C_{th} = \frac{F^{prop}}{1/2\ \rho\ U^2\ \left(1\ -\ w_{prop}\right)^2\ \pi/4\ D_{prop}^2} \tag{68}$$

The rudder-propeller interaction forces in ship-based axes are as follows:

$$F_1^{rudder-prop,S} = F_{drag}^{rudder-prop} \tag{69}$$

$$F_2^{rudder-prop,S} = -F_{lift}^{rudder-prop}\ \sin\Gamma \tag{70}$$

$$F_3^{rudder-prop,S} = F_{lift}^{rudder-prop}\ \cos\Gamma \tag{71}$$

$$F_4^{rudder-prop,S} = \overline{y}^S\ F_3^{rudder-prop,S}\ -\ \overline{z}^S\ F_2^{rudder-prop,S} \tag{72}$$

$$F_5^{rudder-prop,S} = -\left(\overline{x}^S + \overline{c}/4\right)\ F_3^{rudder-prop,S}\ +\ \overline{z}^S\ F_1^{rudder-prop,S} \tag{73}$$

$$F_6^{rudder-prop,S} = \left(\overline{x}^S + \overline{c}/4\right)\ F_2^{rudder-prop,S}\ -\ \overline{y}^S\ F_1^{rudder-prop,S} \tag{74}$$

where $\overline{x}^S, \overline{y}^S, \overline{z}^S$ is the location of the rudder centroid in ship-based axes, and $\overline{c}$ is the mean rudder chord length. Conversion from ship-based axes to translating-earth axes is done using Equations (9) to (14).

When modelling rudder-propeller interaction forces, the greatest uncertainty lies in the selection of the rudder-propeller interaction coefficient $C^{rudder-prop}$. If a large rudder is located immediately aft of a propeller, then the interaction coefficient $C^{rudder-prop}$ can be set to 1.0. Alternatively, if the rudder is clearly not in the propeller slipstream, then the interaction coefficient $C^{rudder-prop}$ can be set to 0.0. For intermediate cases such as typical modern frigates with a single rudder aft of two propellers, it is more difficult to select a suitable interaction coefficient.

10 Rudder and Propeller RPM Control Modelling

Simulation of the motions of a freely maneuvering ship requires modelling of rudder and propeller RPM controls. ShipMo3D uses linear control systems to model both rudder and propeller responses to input commands.

The rudder control system is the same as that presented in Reference 4 for a ship travelling with quasi-steady speed and heading. The rudder response characteristics are modelled as follows:

$$\ddot{\delta}^{rudder} \; + \; 2 \; \zeta_\delta \; \omega_\delta^{rudder} \; \dot{\delta}^{rudder} \; + \; \omega_\delta^2 \; \delta^{rudder} \;\; = \;\; \omega_\delta^2 \; \delta_C^{rudder} \tag{75}$$

where $\ddot{\delta}^{rudder}$ is rudder acceleration, ζ_δ is the nondimensional damping response constant, ω_δ is the rudder response natural frequency, $\dot{\delta}^{rudder}$ is rudder velocity, and δ_C^{rudder} is command rudder angle. The rudder motions in the time domain are easily evaluated as follows:

$$\ddot{\delta}^{rudder} \;\; = \;\; \omega_\delta^2 \;\; \left(\delta_C^{rudder} \; - \delta^{rudder} \right) - \; 2 \; \zeta_\delta \; \omega_\delta \; \dot{\delta}^{rudder} \tag{76}$$

The autopilot for a freely maneuvering ship is very similar to the autopilot for a ship with quasi-steady speed and heading presented in Reference 4. The main difference is that an autopilot for a freely maneuvering ship uses input motions in earth-fixed axes, while an autopilot for a ship with quasi-steady speed and heading uses input motions in translating earth axes. Consequently, yaw gains for a freely maneuvering autopilot are of opposite sign to those for an autopilot based on translating earth axes.

The command rudder angle for a freely maneuvering autopilot is given by:

$$\delta_C^{rudder} \;\; = \;\; \sum_{j=1}^{6} \left[k_{\delta j}^a \; \ddot{\eta}_j^f \; + \; k_{\delta j}^v \; \dot{\eta}_j^f \; + \; k_{\delta j}^d \; \left(\eta_j^f \; - \; \eta_{Cj}^f \right) \right] \tag{77}$$

where $k_{\delta j}^a$ is the acceleration gain for motion mode j, $k_{\delta j}^v$ is the velocity gain, $k_{\delta j}^d$ is the displacement gain, and η_{Cj}^f is the command displacement.

The simulation of a rudder control system including autopilot requires selection of suitable input values. For a US Coast Guard cutter representative of modern frigate design, Smith [19] indicates a maximum rudder deflection of 35 degrees and maximum rudder rate of 3 degrees per second. For modelling of a conventional downward rudder using ShipMo3D, the yaw gain and yaw velocity gain for a freely maneuvering autopilot will typically have values less than zero.

The propeller control system is modelled very similarly to the rudder control system, with the rate of change of propeller RPM being modelled as follows:

$$\ddot{RPM}^{prop} = \omega_{RPM}^2 \, (RPM_C^{prop} - RPM^{prop}) - 2\,\zeta_{RPM}\,\omega_{RPM}\,\dot{RPM}^{prop} \qquad (78)$$

where $\ddot{RPM}^{prop}$ is the second derivative with respect to time of propeller RPM, ω_{RPM} is the RPM response natural frequency, RPM_C^{prop} is command propeller RPM, RPM^{prop} is propeller RPM, ζ_{RPM} is RPM response damping, and $\dot{RPM}^{prop}$ is the first derivative with respect to time of propeller RPM.

11 Validation of Turning Circles for Esso Osaka Tanker

Initial validation of ShipMo3D maneuvering predictions has been done using turning circles for the oil tanker Esso Osaka, with particulars as given in Table 2. Crane [20] describes a comprehensive set of maneuvering trials conducted for the Esso Osaka. The high quality of the reported trials data has prompted much subsequent work on prediction of maneuvering forces and motions for the Esso Osaka. A recent Special Committee of the International Towing Tank Conference [6] has produced an excellent overview on maneuvering forces and motions for the Esso Osaka.

Table 2: *Main Particulars for the Esso Osaka During Maneuvering Trials*

Length, L (between perpendiculars)	325 m
Beam, B	53 m
Midships draft, T_{mid}	21.73 m
Trim by stern, t_{stern}	0.0 m
Displacement, $\triangle$	319,400 tonnes
Longitudinal CG forward of midship	10.3 m

Esso Osaka geometric data provided by Crane were used to develop ShipMo3D input. Detailed resistance and propulsion data were not found; thus, it was necessary to estimate these characteristics. Resistance coefficients were taken from the Series 60 hull with $C_B = 0.80$ [21], which has geometric properties very similar to the Esso Osaka (see Table 3). Table 4 shows the resulting estimated resistance coefficients scaled to speeds for the Esso Osaka.

For propulsion characteristics of the Esso Osaka, Crane indicates that the propeller diameter D_{prop} is 9.1 m and that the propeller rotates at 51 RPM when the ship

travels at 10 knots in calm water. Based on data given in Reference 16, the wake fraction w_{prop} was estimated to be 0.352 and the thrust deduction coefficient t_{prop} was estimated to be 0.2. To obtain a thrust coefficient curve for the Esso Osaka, it was decided that the sample thrust coefficient curve from Figure 6 could be scaled to provide a thrust equivalent to the modelled resistance of the Esso Osaka at 10 knots. Surprisingly, the sample thrust coefficient curve provided a thrust within 2 percent of the required value, with the final scaled thrust coefficient curve for the Esso Osaka being as follows:

$$K_T \;=\; 0.394 \;-\; 0.197\, J_{prop} \;-\; 0.148\, J_{prop}^2 \tag{79}$$

Table 5 gives rudder dimensions and modelled control properties for the Esso Osaka. The rudder span and chord are taken from Reference 20. With the exception of maximum rudder deflection δ_{max}^{rudder}, the rudder control parameters are estimates based on published values for other ships. The rudder-propeller interaction coefficient $C^{rudder-prop}$ is estimated to be 0.9 due to the proximity and large size of the rudder relative to the propeller.

Figures 7 to 12 present predicted and measured turning circle data for the Esso Osaka with initial velocities of 10 knots and 7.7 knots. The ShipMo3D predictions use hull maneuvering coefficients based on Inoue et al. [10]. The predictions show generally good agreement with the sea trials data. The most noticeable differences are that the predicted ship speeds and absolute yaw rates are larger than actual values when the ship reaches its steady-state turning condition. When examining the sea trial data, the data for an initial ship speed of 7.7 knots are less consistent than the data for 10 knots. The lesser consistency at lower ship speed is likely due to the ship being more prone to environmental forces such as those from winds and currents.

The present ShipMo3D predictions for maneuvering of the Esso Osaka are encouraging. The final turning circle diameter for the Esso Osaka is equal to only 3 ship lengths; thus, nonlinear effects are significant.

Table 3: *Principal Hull Coefficients for Esso Osaka and Series 60 Hull with $C_B = 0.80$*

	Esso Osaka	Series 60 with $C_B = 0.80$
Block coefficient C_B	0.831	0.80
Length/beam L/B	6.1	6.5
Beam/draft B/T	2.4	2.5
Length L	325 m	122 m

Table 4: *Estimated Resistance Cofficients for Esso Osaka*

Speed (knots)	Resistance coefficient $C_{Dx} = F/(1/2\rho U^2 A_w)$
2.0	0.00306
16.0	0.00306
18.0	0.00308
19.6	0.00328
21.2	0.00370
22.9	0.00426

Table 5: *Rudder Dimensions and Modelled Control Properties for Esso Osaka*

Rudder span s_{rudder}	13.85 m
Rudder chord length c_{rudder}	9.00 m
Maximum rudder deflection δ_{max}^{rudder}	35 degrees
Maximum rudder velocity $\dot{\delta}_{max}^{rudder}$	3 deg/s
Response natural frequency ω_δ	3 rad/s
Response damping ζ_δ	0.85
Rudder-propeller interaction coefficient $C^{rudder-prop}$	0.9

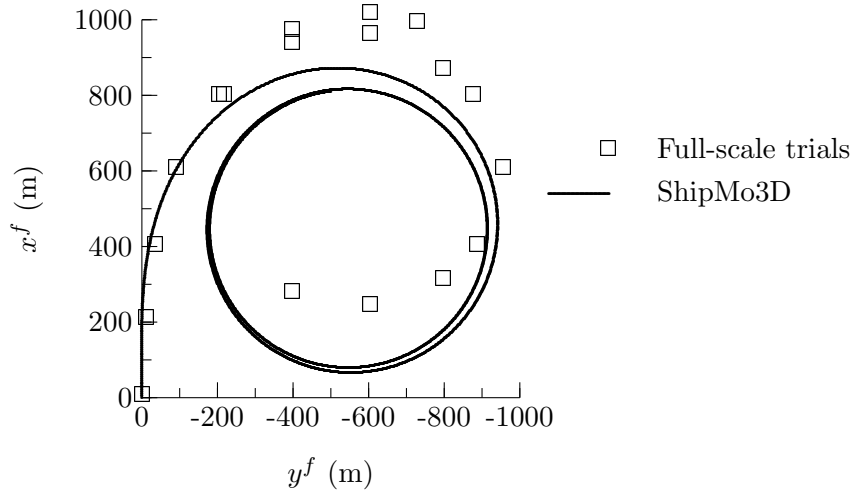

Figure 7: *Turning Circle Trajectory for Esso Osaka Starboard Turn at 10 Knots with 35 degree Rudder*

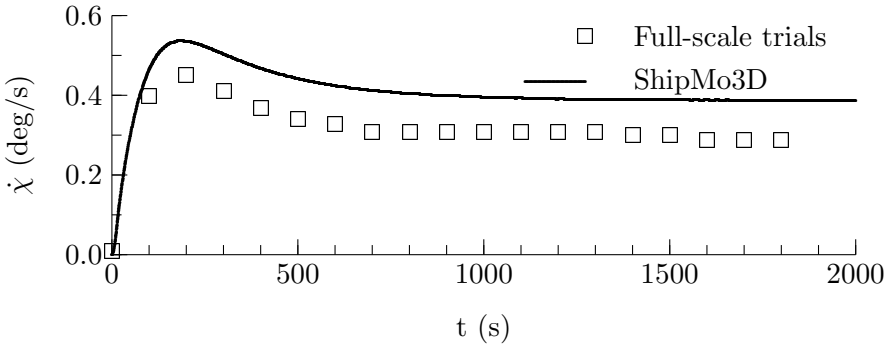

Figure 8: *Yaw Rate Versus Time for Esso Osaka Starboard Turn at 10 Knots with 35 degree Rudder*

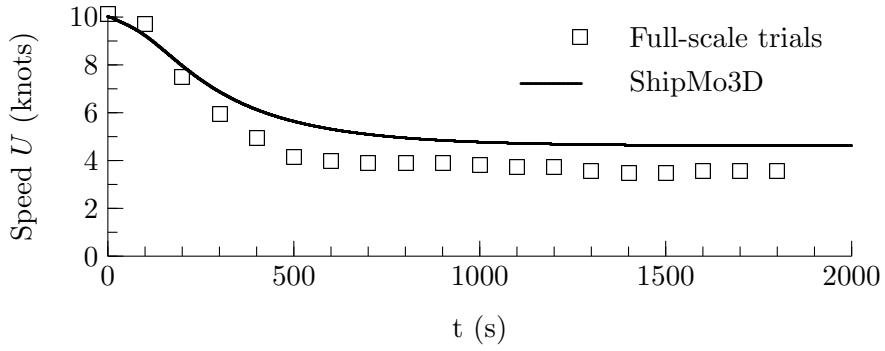

Figure 9: *Ship Speed Versus Time for Esso Osaka Starboard Turn at 10 Knots with 35 degree Rudder*

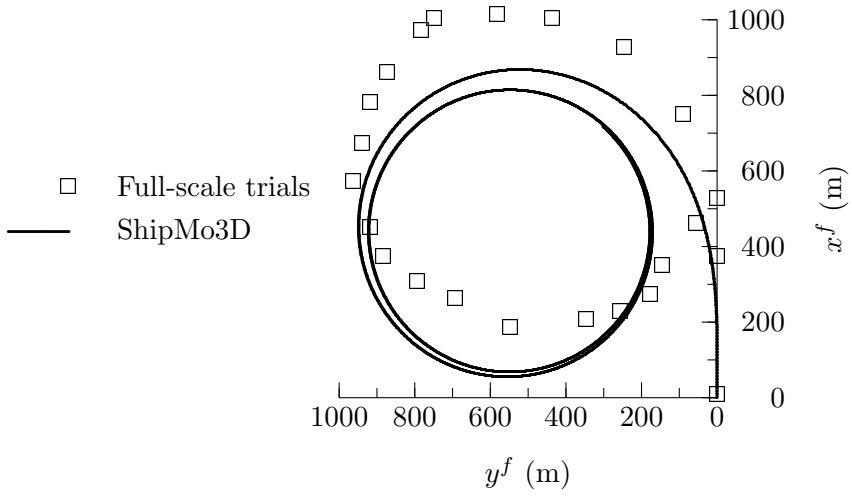

Figure 10: *Turning Circle Trajectory for Esso Osaka Port Turn at 7.7 Knots with 35 degree Rudder*

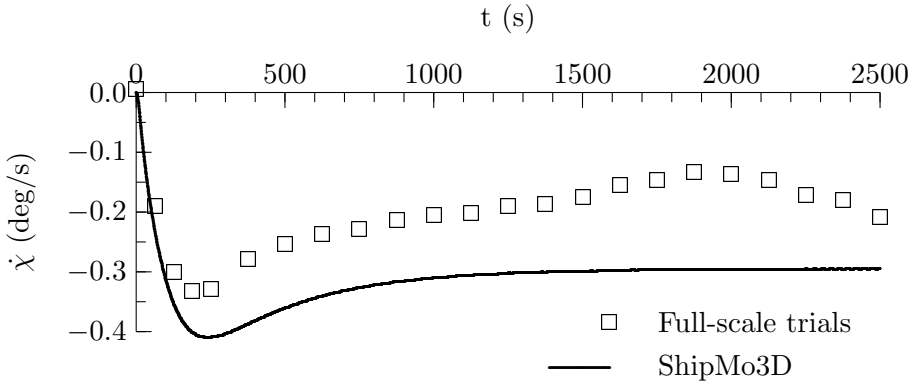

Figure 11: *Yaw Rate Versus Time for Esso Osaka Port Turn at 7.7 Knots with 35 degree Rudder*

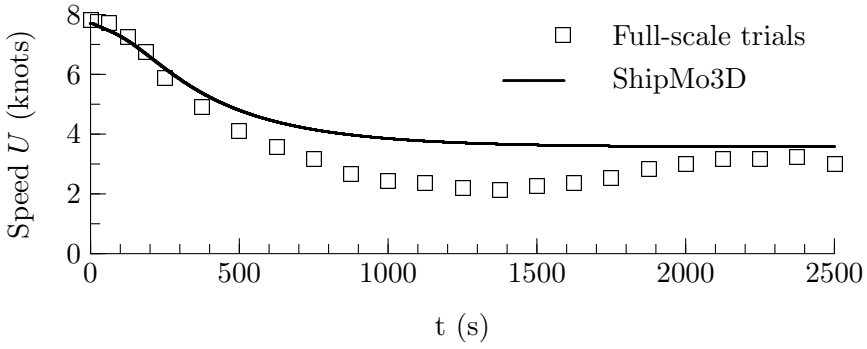

Figure 12: *Ship Speed Versus Time for Esso Osaka Port Turn at 7.7 Knots with 35 degree Rudder*

12 Unclassified Maneuvering Modelling of HALIFAX

Examination of predicted maneuvering forces and motions for Canada's HALIFAX class frigate can provide useful insight into maneuvering prediction of naval vessels. Measured maneuvering data for HALIFAX are classified and not presented here. Similarly, measured resistance and propulsion data for HALIFAX are classified; thus, resistance and propulsion properties are modelled using approximations based on data in the open literature.

Table 6 gives main particulars for the HALIFAX with the loading condition based on that used for model tests with the CPF hydroelastic model [22]. Resistance coefficients given in Table 7 have been estimated based on values in Schmitke and Murdey [23] for a frigate with similar geometry. The tabulated resistance coefficients are intended to encompass all possible operating speeds.

Based on the geometry of the propeller shaft brackets for HALIFAX, the two HALIFAX propellers are modelled with propellers having nominal diameters of 5.6 m. The propeller wake fraction and thrust deduction coefficient are both assumed to be 0.0 based on comments regarding destroyer type vessels in Reference 16. The propeller thrust coefficient curve has been designed based on the following constraints:

- For a nominal ship speed of 30 knots, the propeller RPM should be a suitable nominal value (e.g., 100),
- The propeller thrust coefficient curve is scaled from the curve $K_t(J_{prop}) = 0.40 - 0.2J_{prop} - 0.15J_{prop}^2$ from Reference 16,
- To ensure operation of the propeller at a realistic advance ratio, the advance ratio at a ship speed of 35 knots is less than 0.90,
- At zero advance coefficient, the thrust coefficient curve should satisfy $0.2 \leq K_t(J_{prop} = 0) \leq 0.6$.

The following thrust coefficient curve for the HALIFAX propellers gives a nominal speed of 30 knots for the propellers rotating at 200 RPM:

$$K_T(J_{prop}) \;=\; 0.32 \;-\; 0.16\, J_{prop} \;-\; 0.12\, J_{prop}^2 \tag{80}$$

Table 8 gives speeds in calm water and associated propeller RPM values determined using iterative solution.

Table 9 gives modelled rudder control properties and the estimated rudder-propeller interaction coefficient for the HALIFAX. With the exception of maximum rudder

Table 6: *Main Particulars for HALIFAX Class Frigate, CPF Hydroelastic Model Deep Departure Condition*

Length, L	124.5 m
Beam, B	14.8 m
Midships draft, T_{mid}	4.97 m
Trim by stern, t_{stern}	-0.04 m
Displacement, $\triangle$	4601 tonnes (salt water)
Vertical centre of gravity, $\overline{KG}$	6.26 m
Dry roll radius of gyration r_{xx}	5.82 m
Dry pitch radius of gyration r_{yy}	28.8 m
Dry yaw radius of gyration r_{zz}	28.8 m

Table 7: *Resistance Coefficients for Unclassified Modelling of HALIFAX Maneuvering*

Speed (knots)	Resistance Coefficient $C_R = F_R/(1/2\rho U^2 A_w)$
≤ 10	0.0040
15	0.0042
20	0.0057
25	0.0069
30	0.0099
35	0.0108

Table 8: *Ship Speeds in Calm Water and Associated Propeller RPM for Unclassified Modelling of HALIFAX Maneuvering*

Speed (knots)	Propeller RPM
5	28.9
10	57.7
15	87.1
20	121.0
25	156.0
30	200.4

Table 9: *Rudder Control Properties for HALIFAX*

Maximum rudder deflection δ_{max}^{rudder}	35 degrees
Maximum rudder velocity $\dot{\delta}_{max}^{rudder}$	3 deg/s
Response natural frequency ω_δ	3 rad/s
Response damping ζ_δ	0.85
Rudder-propeller interaction coefficient $C^{rudder-prop}$	0.5

Table 10: *Predicted Maneuvering Coefficients for HALIFAX*

Y'_v	-0.207
Y'_r	0.062
N'_v	-0.080
N'_r	-0.037
$Y'_{v\|v\|}$	-1.006
$Y'_{v\|r\|}$	-0.140
$Y'_{r\|r\|}$	0.000
N'_{vr^2}	0.000
$N'_{r\|r\|}$	-0.060
N'_{rv^2}	-0.200

deflection δ_{max}^{rudder}, the rudder control parameters are estimates based on published values for other ships.

Table 10 gives predicted hull maneuvering coefficients for HALIFAX determined using Equations (27) to (43).

Figures 13 to 15 show the trajectory, yaw rate, and speed for HALIFAX executing a starboard turning circle at an initial speed of 25 knots and 30 degree rudder angle. Table 11 gives associated turning circle statistics.

When simulating maneuvers of existing ships, hull maneuvering coefficients are often adjusted to provide improved agreement between observed and predicted maneuvers. To examine the influence of hull maneuvering coefficients on predicted turning circle properties, simulations have been conducted for which predicted hull maneuvering coefficient have been incremented by the range of uncertainty as given in Table 1. Tables 12 and 13 show the predicted variations to turning circle properties. Turning circle properties are most responsive to changes in the linear yaw-yaw maneuvering

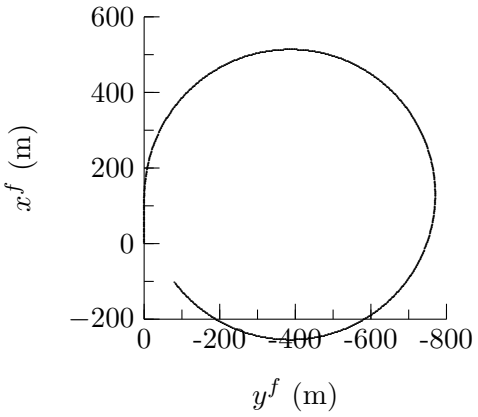

Figure 13: *Turning Circle Trajectory for HALIFAX Starboard Turn at 25 Knots with 30 Degree Rudder*

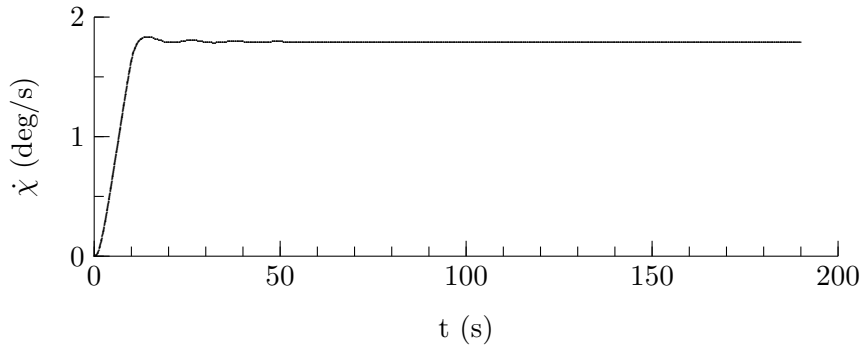

Figure 14: *Yaw Rate Versus Time for HALIFAX Starboard Turn at 25 Knots with 30 Degree Rudder*

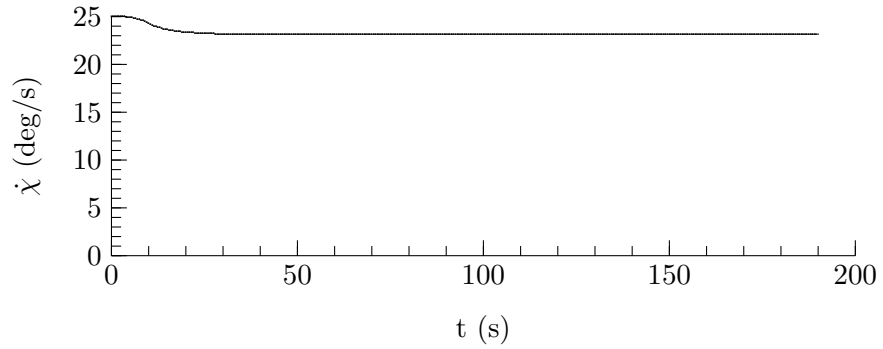

Figure 15: *Ship Speed Versus Time for HALIFAX Starboard Turn at 25 Knots with 30 Degree Rudder*

Table 11: *Properties of Predicted HALIFAX Starboard Turning Circle at 25 Knots with 30 Degree Rudder*

Transfer	341 m
Advance	511 m
Tactical diameter	768 m
Final diameter	768 m
Final yaw velocity	1.79 m/s
Final speed	23.2 knots

coefficient N'_r. Variation of the other yaw force coefficients N'_α and $N'_{r'|r'|}$ also has a significant influence on turning circle properties. Final speed for HALIFAX varies by less than 0.5 percent for variation of each hull maneuvering coefficient.

Predicted turning circle characteristics will also vary with the selected value of the rudder-propeller interaction coefficient, which can be difficult to assess accurately. Table 14 indicates that turning circle properties can vary by approximately 10 percent when the rudder-propeller interaction coefficient is varied by 0.3 relative to its reference value of 0.5.

Table 12: *Variation of HALIFAX Turning Circle Properties with Increases to Hull Maneuvering Coefficients, 25 Knots with 30 Degree Rudder*

		Percentage change in turning circle property					
Maneuver coef.	Coef. increment	Tactical diameter	Advance	Transfer	Final diameter	Final yaw rate	Final speed
Y'_v	0.05	0	0	-1	0	0	0
Y'_r	0.05	1	-1	4	1	-1	0
N'_v	0.02	7	5	7	7	-6	0
N'_r	0.02	-16	-14	-16	-16	19	0
$Y'_{v\|v\|}$	0.20	0	0	-1	0	0	0
$Y'_{v\|r\|}$	0.20	0	0	-2	0	1	0
$Y'_{r\|r\|}$	0.05	0	0	1	0	0	0
N'_{vr^2}	0.05	2	1	2	2	-2	0
$N'_{r\|r\|}$	0.02	-6	-4	-6	-6	6	0
N'_{rv^2}	0.20	-2	-2	-2	-2	3	0

Table 13: *Variation of HALIFAX Turning Circle Properties with Decreases to Hull Maneuvering Coefficients, 25 Knots with 30 Degree Rudder*

		Percentage change in turning circle property					
Maneuver coef.	Coef. increment	Tactical diameter	Advance	Transfer	Final diameter	Final yaw rate	Final speed
Y'_v	-0.05	0	0	1	0	0	0
Y'_r	-0.05	-1	1	-3	-1	1	0
N'_v	-0.02	-6	-4	-6	-6	6	0
N'_r	-0.02	17	14	17	17	-15	0
$Y'_{v\|v\|}$	-0.20	0	0	1	0	0	0
$Y'_{v\|r\|}$	-0.20	0	0	1	0	-1	0
$Y'_{r\|r\|}$	-0.05	0	0	-1	0	0	0
N'_{vr^2}	-0.05	-2	-1	-2	-2	2	0
$N'_{r\|r\|}$	-0.02	5	4	5	5	-5	0
N'_{rv^2}	-0.20	2	2	2	2	-2	0

Table 14: *Variation of HALIFAX Turning Circle Properties with Changes to Rudder-Propeller Interaction Coefficient $C^{rudder-prop}$, 25 Knots with 30 Degree Rudder*

$C^{rudder-prop}$	Percentage change relative to $C^{rudder-prop} = 0.5$					
	Tactical diameter	Advance	Transfer	Final diameter	Final yaw rate	Final speed
0.20	12	9	13	12	-12	-2
0.80	-8	-6	-9	-8	11	1

13 Validation of Motions in Waves for Steered Warship Model on Straight Course

Previous validation for ShipMo3D [4, 24] has shown very good agreement with experimental motions for ships travelling at steady speed and heading in waves. The introduction of hull maneuvering forces to ShipMo3D necessitates new validation of predictions in the frequency and time domain for a ship assumed to have quasi-steady speed and heading. Furthermore, the new ShipMo3D capability for modelling freely maneuvering ships requires validation of predicted motions in waves.

This section presents validation of motions in waves for the steered warship model of Lloyd and Crossland [25], which was used for previous ShipMo3D validation in Reference 4. The validation includes numerical predictions in the frequency and time domains for a ship with quasi-steady speed and heading, and in the time domain for a freely maneuvering ship. All predictions include the new ShipMo3D hull maneuvering forces. The predictions for a freely maneuvering ship also include forces due to viscous resistance, propeller thrust, and rudder-propeller interaction. The hull maneuvering forces are estimated based on Section 4. For the predictions assuming quasi-steady speed and heading, the nonlinear maneuvering force terms are assumed to be zero. Table 15 gives resistance coefficients for the steered warship model estimated using Schmitke and Murdey [23]. The two propellers are assumed to have a diameter of 0.2 m and the thrust coefficient curve as follows based on Figure 16 of Reference 16:

$$K_T(J_{prop}) \;=\; 0.40 \;-\; 0.20\, J_{prop} \;-\; 0.15 J_{prop}^2 \tag{81}$$

Each of the two rudders is located behind a propeller. The interaction between each rudder and its nearby propeller is modelled using a propeller interaction coefficient $C^{rudder-prop}$ value of 0.9.

In the previous validation work of Reference 4, extra stiffness and damping for surge and sway were introduced to ensure stationkeeping for numerical predictions during low encounter frequencies. In the present validation, these extra stiffness and damping terms are removed to ensure consistency with experimental conditions. Instead, no numerical predictions are made when the non-dimensional encounter frequency $\omega_e \sqrt{L/g}$ is less than 0.24.

Figures 17 to 32 show comparisons between predicted and experimental motions. Agreement between predicted and experimental motions is generally very good. The frequency domain and time domain predictions assuming quasi-steady speed and heading give very similar results. The predictions for a freely maneuvering ship are slightly different from those assuming quasi-steady speed and heading, likely

Table 15: *Resistance Coefficients for Steered Warship Model*

Froude number	Resistance Coefficient $C_R = F_R/(1/2\rho U^2 A_w)$
≤ 0.150	0.0040
0.225	0.0042
0.300	0.0057
0.375	0.0069
0.450	0.0099
0.525	0.0108

because of the inclusion of nonlinear maneuvering forces and rudder-propeller interaction forces for the freely maneuvering ship.

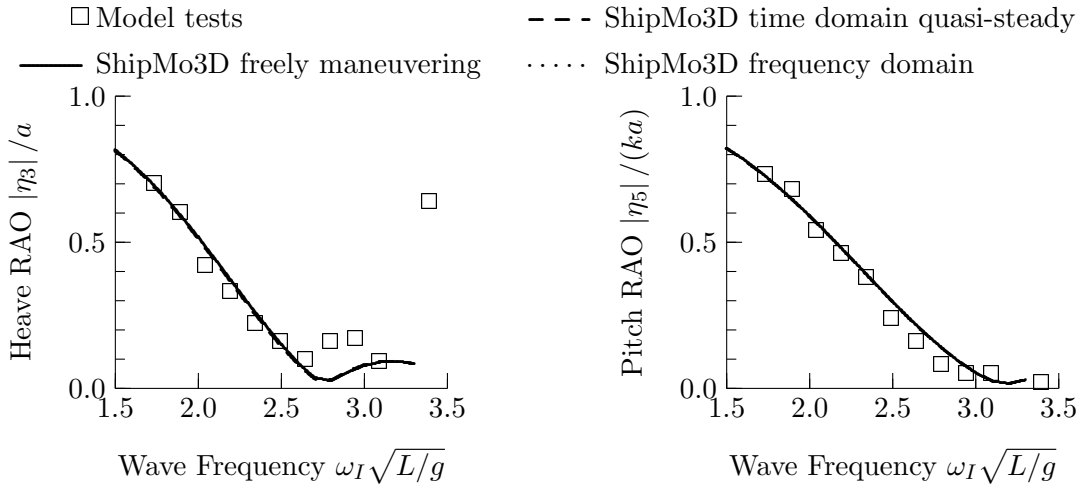

Figure 16: *RAOs for Steered Warship, Stern Quartering Seas at 0 degrees, Froude Number 0.28*

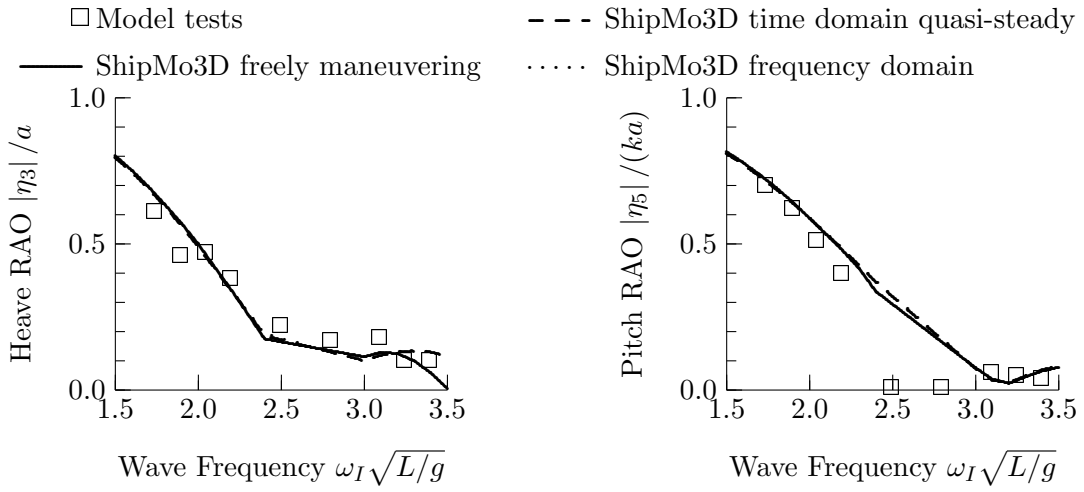

Figure 17: *RAOs for Steered Warship, Stern Quartering Seas at 0 degrees, Froude Number 0.37*

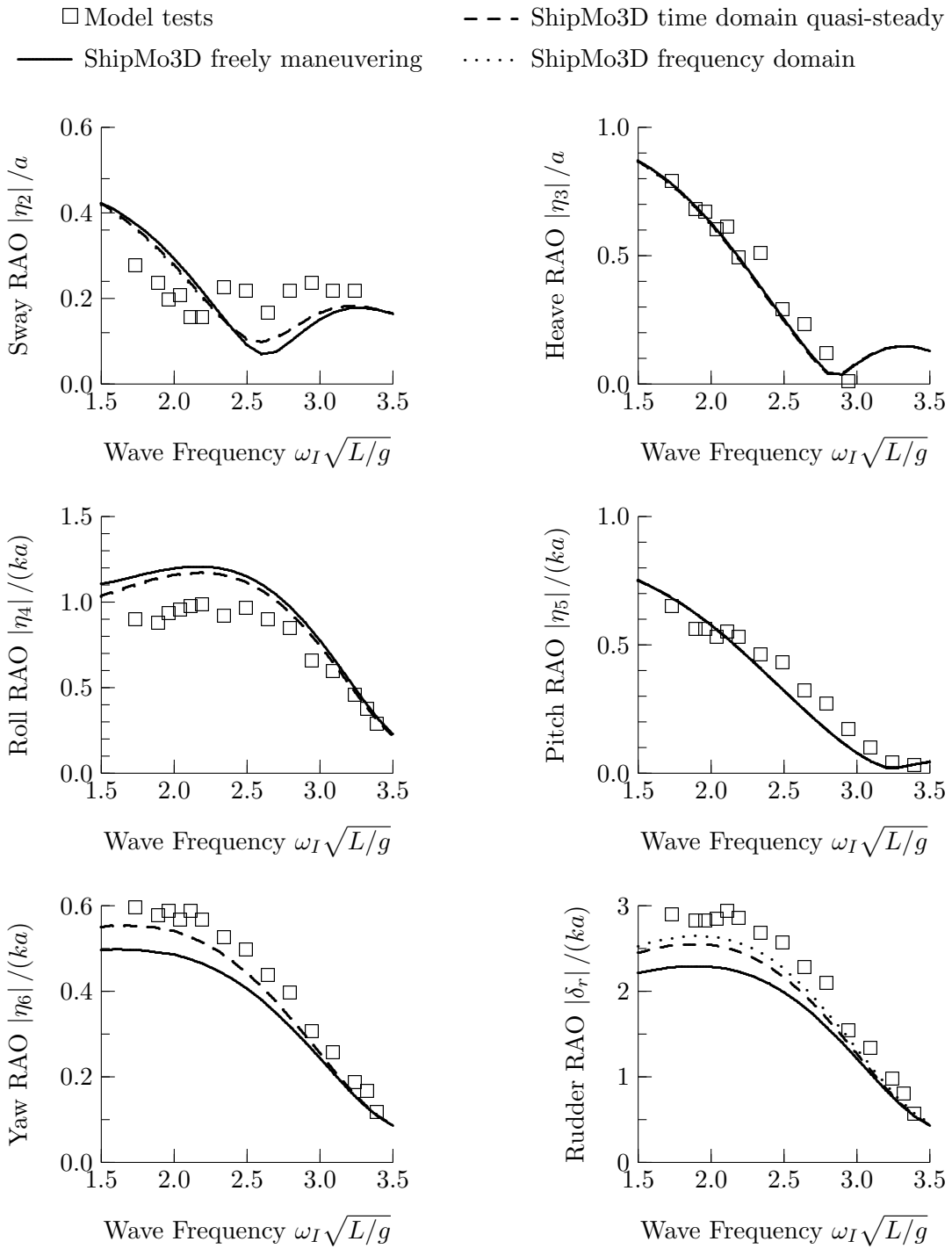

Figure 18: *RAOs for Steered Warship, Stern Quartering Seas at 30 degrees, Froude Number 0.18*

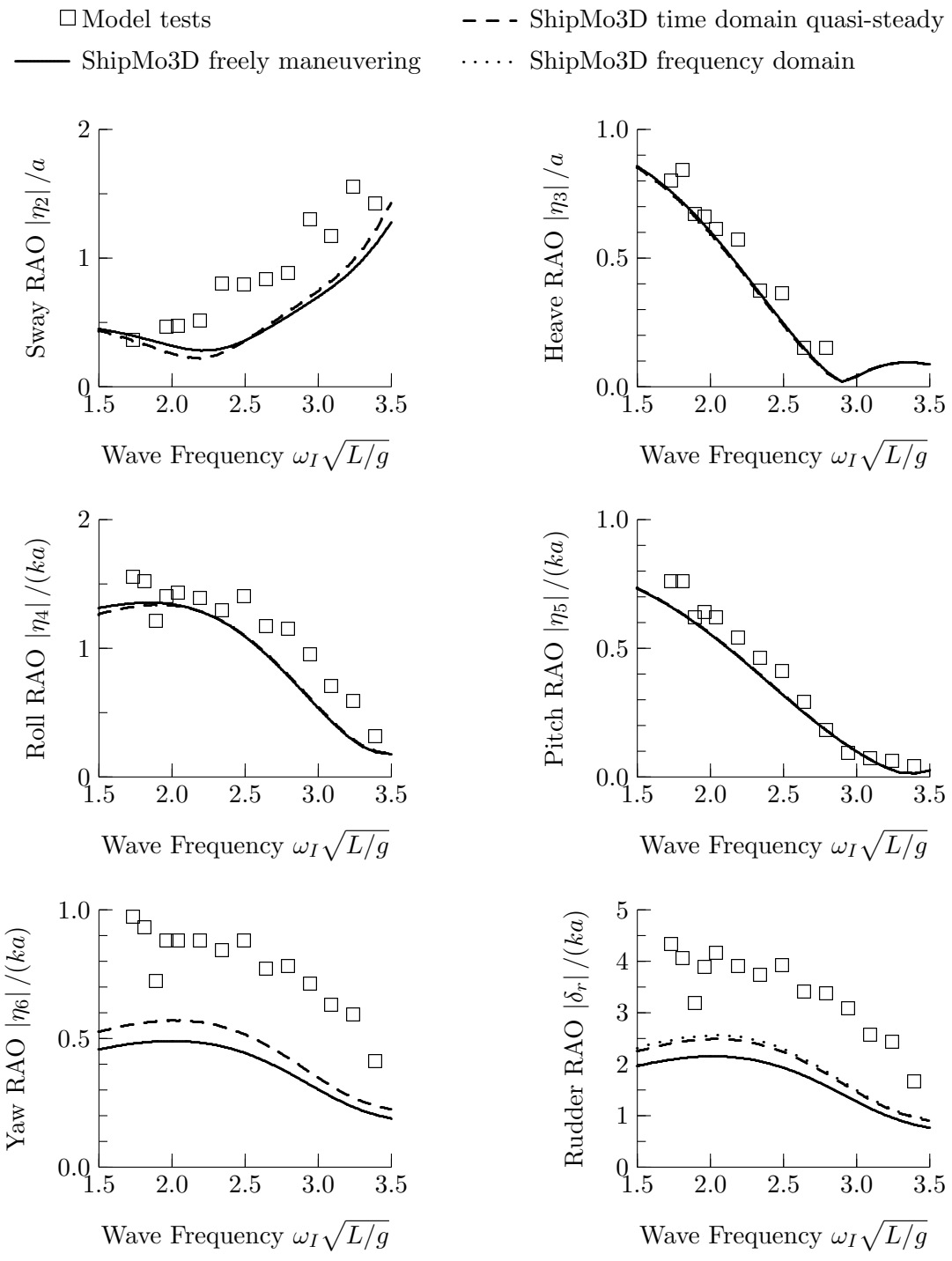

Figure 19: *RAOs for Steered Warship, Stern Quartering Seas at 30 degrees, Froude Number 0.27*

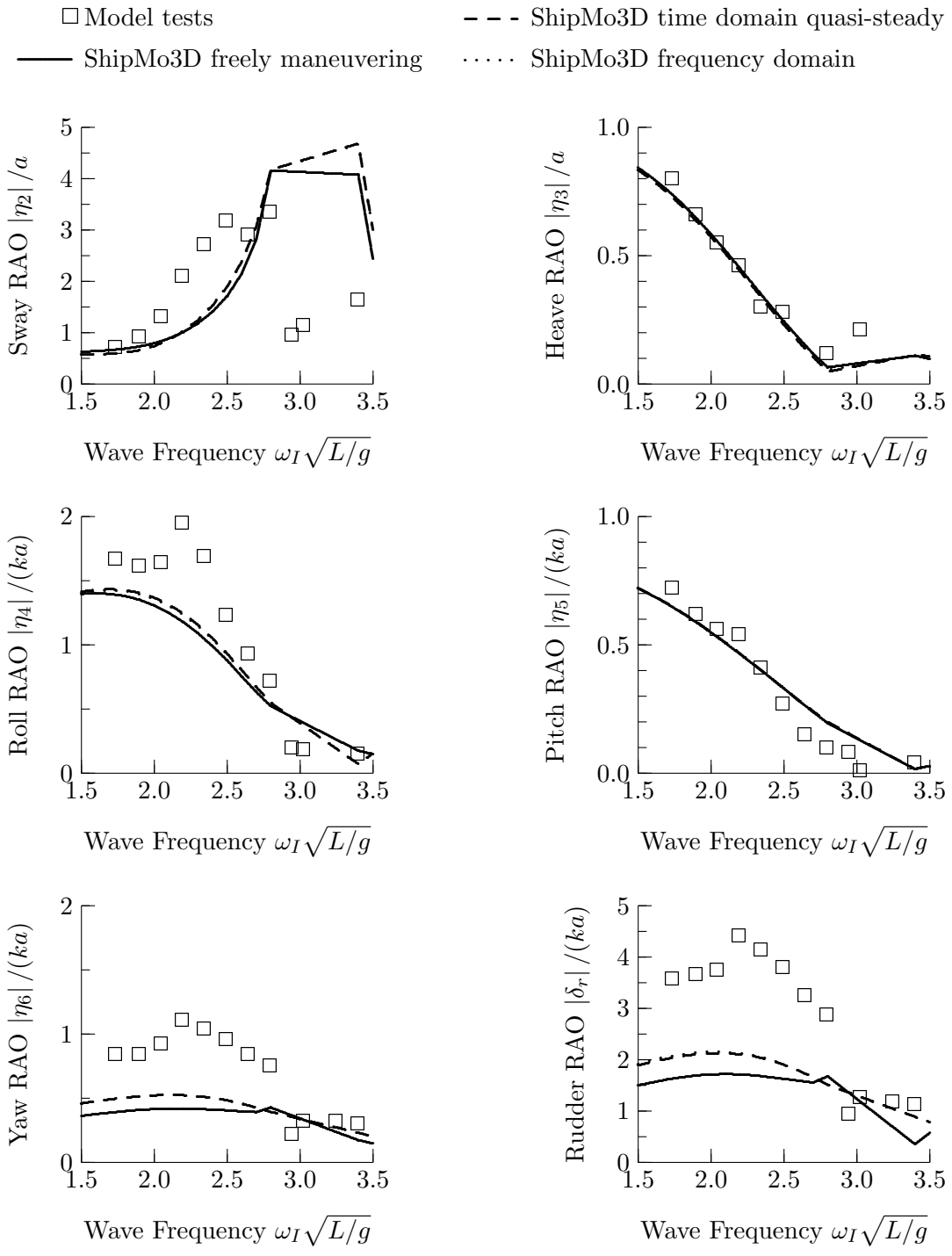

Figure 20: *RAOs for Steered Warship, Stern Quartering Seas at 30 degrees, Froude Number 0.37*

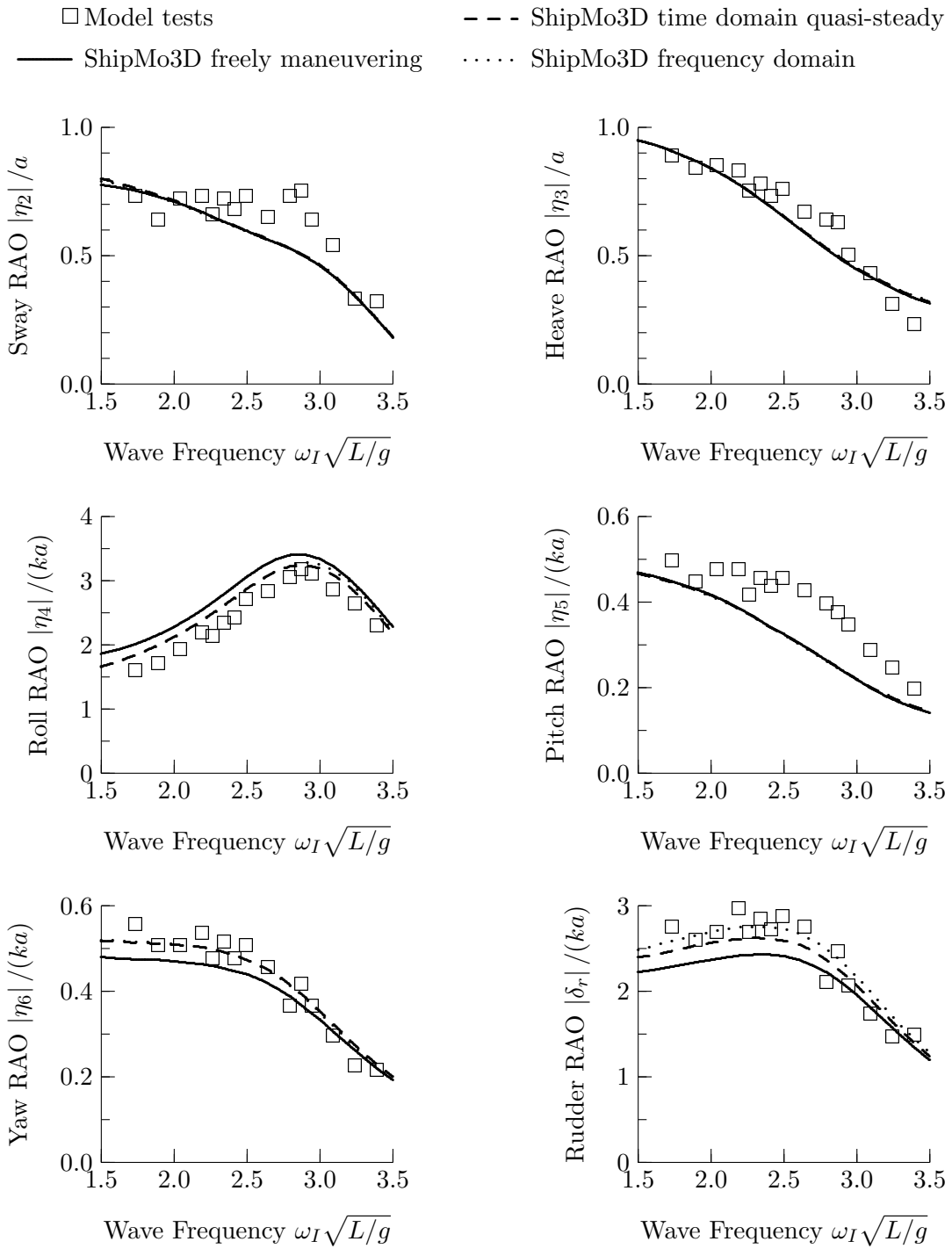

Figure 21: *RAOs for Steered Warship, Stern Quartering Seas at 60 degrees, Froude Number 0.18*

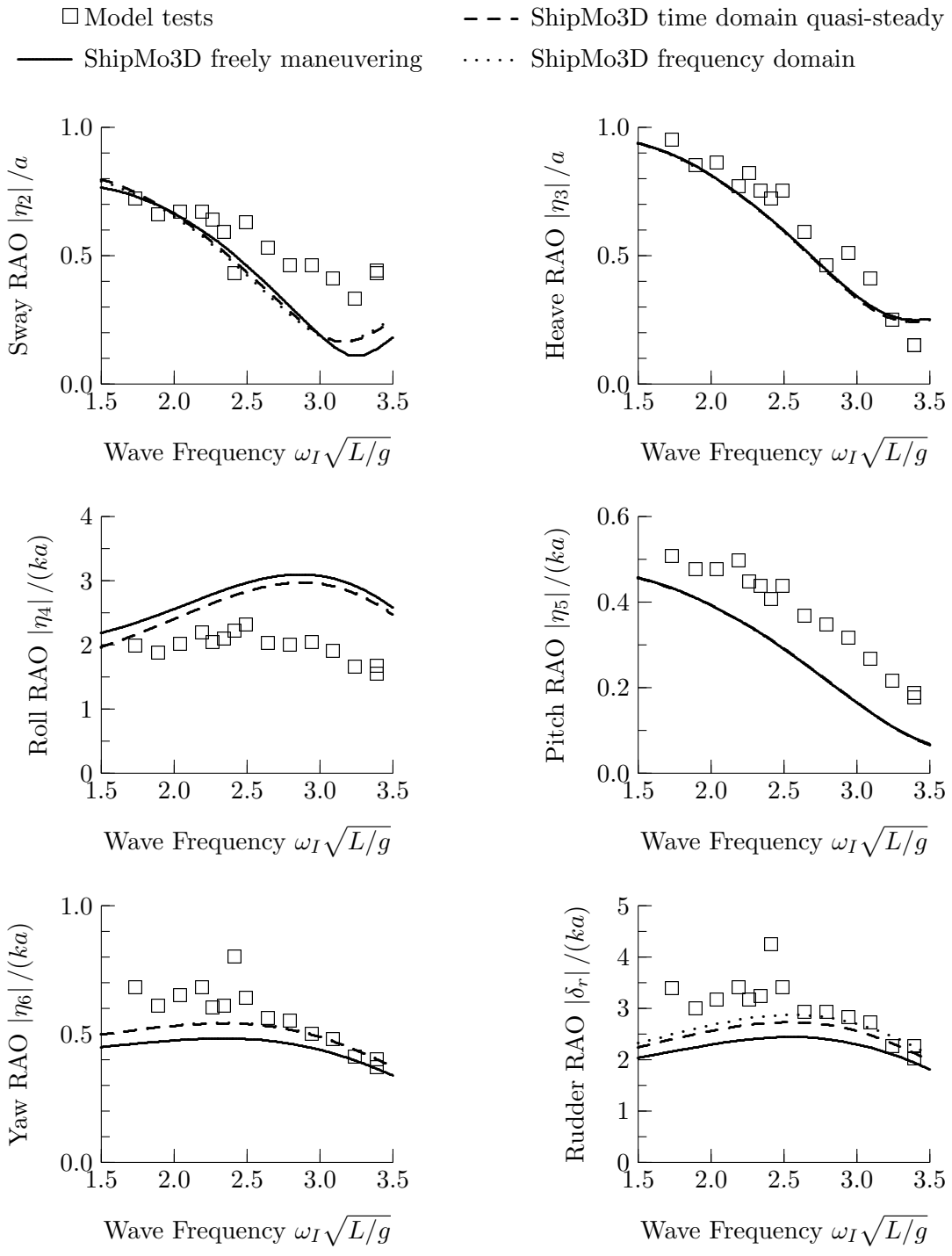

Figure 22: *RAOs for Steered Warship, Stern Quartering Seas at 60 degrees, Froude Number 0.27*

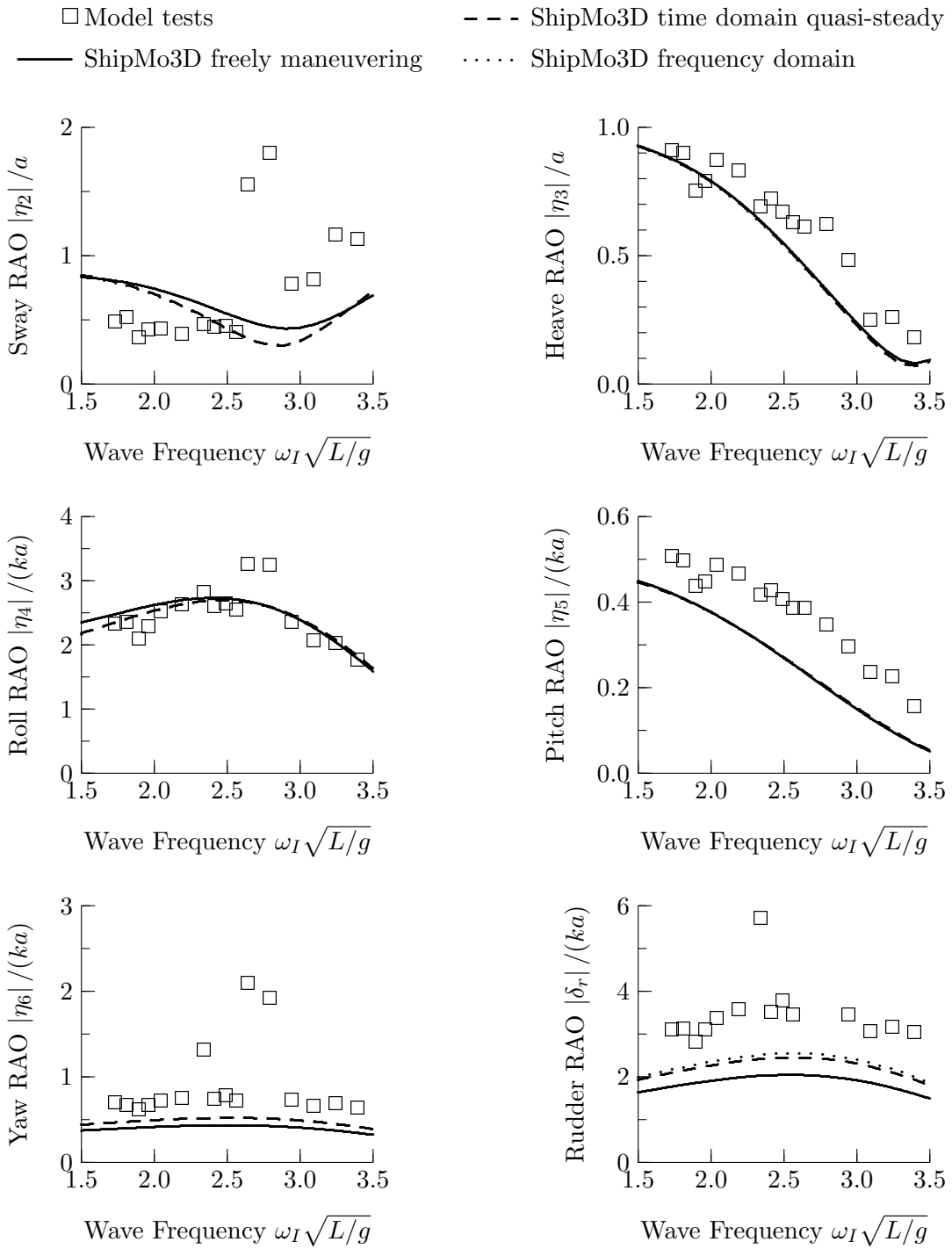

Figure 23: *RAOs for Steered Warship, Stern Quartering Seas at 60 degrees, Froude Number 0.36*

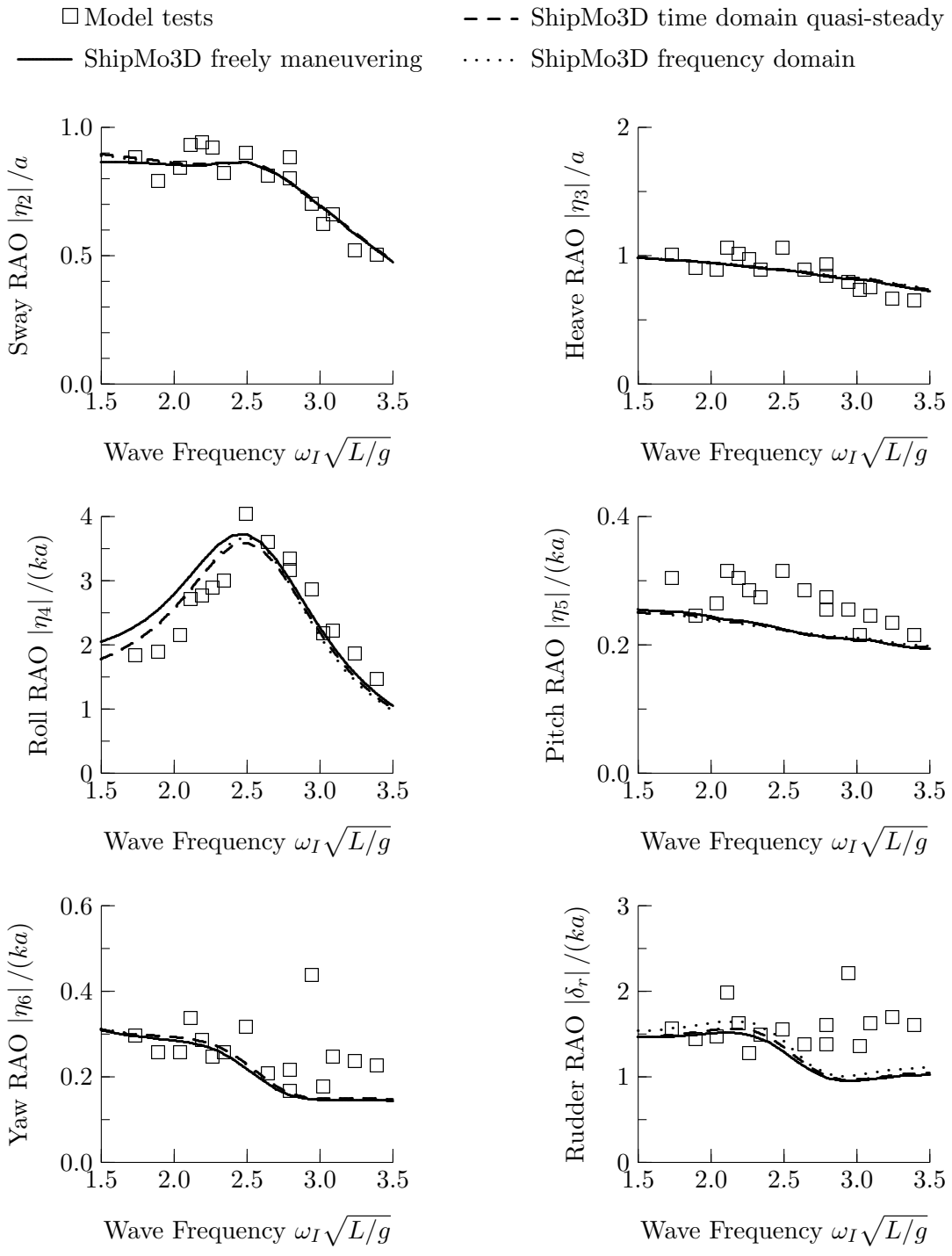

Figure 24: *RAOs for Steered Warship, Stern Quartering Seas at 75 degrees, Froude Number 0.18*

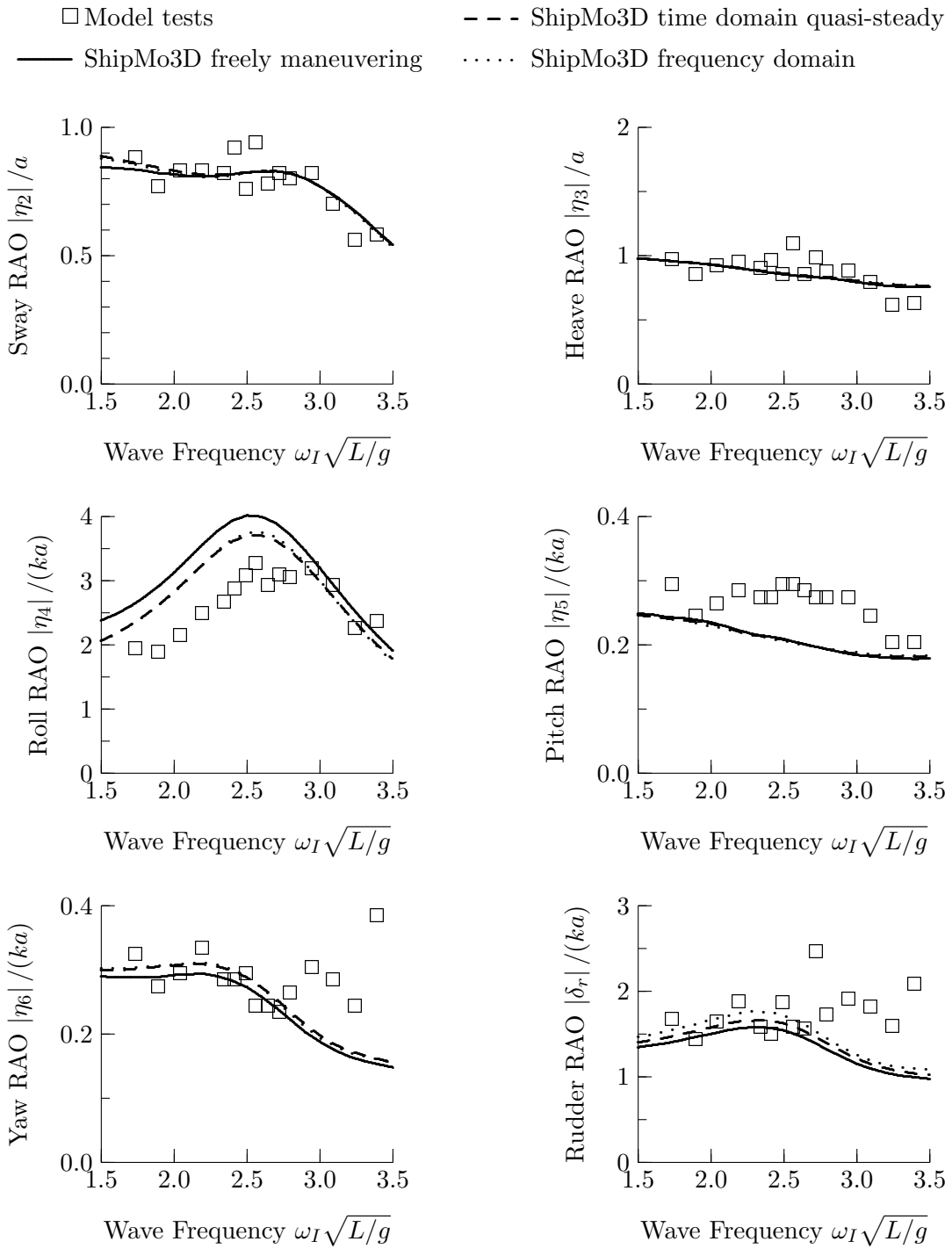

Figure 25: *RAOs for Steered Warship, Stern Quartering Seas at 75 degrees, Froude Number 0.28*

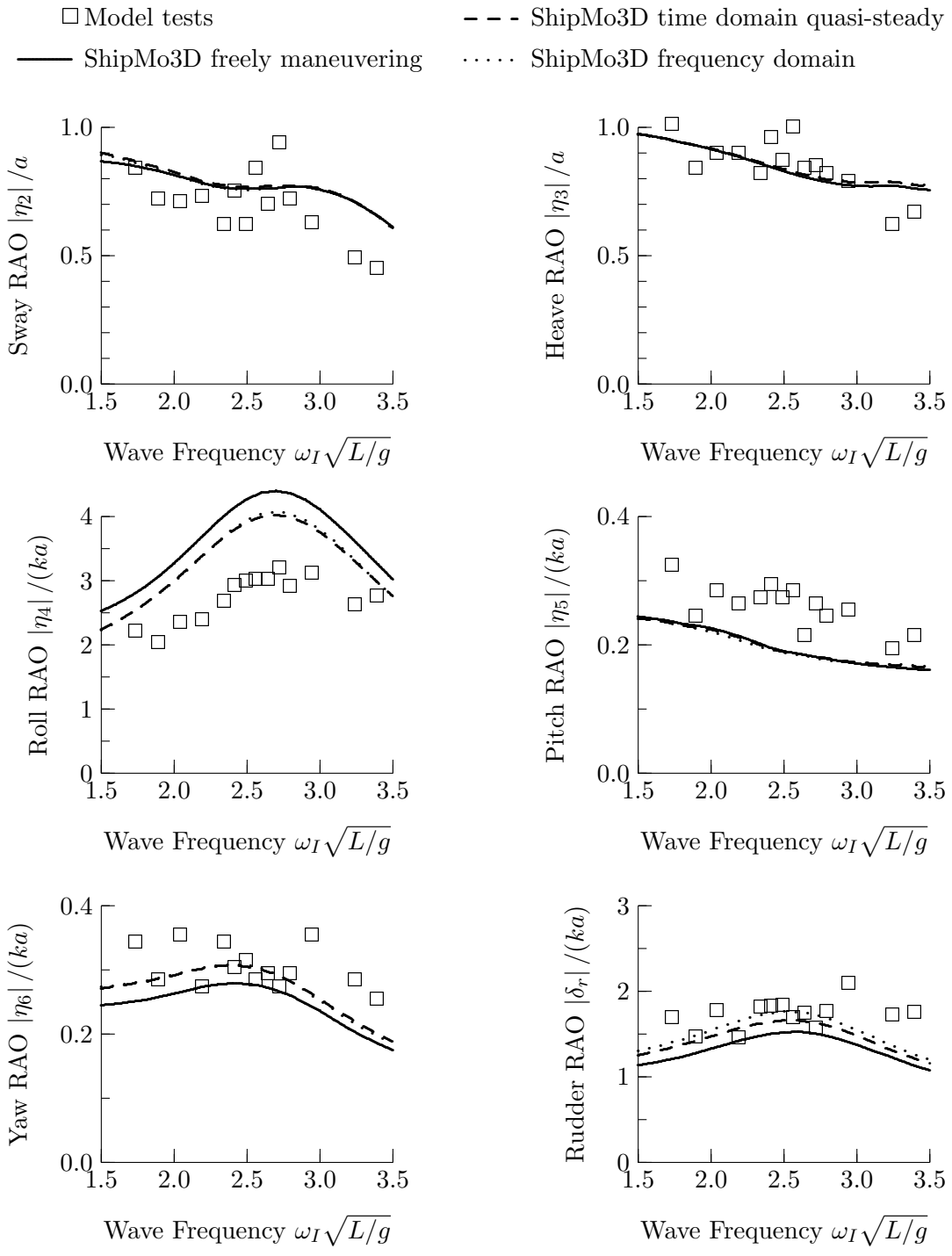

Figure 26: *RAOs for Steered Warship, Stern Quartering Seas at 75 degrees, Froude Number 0.36*

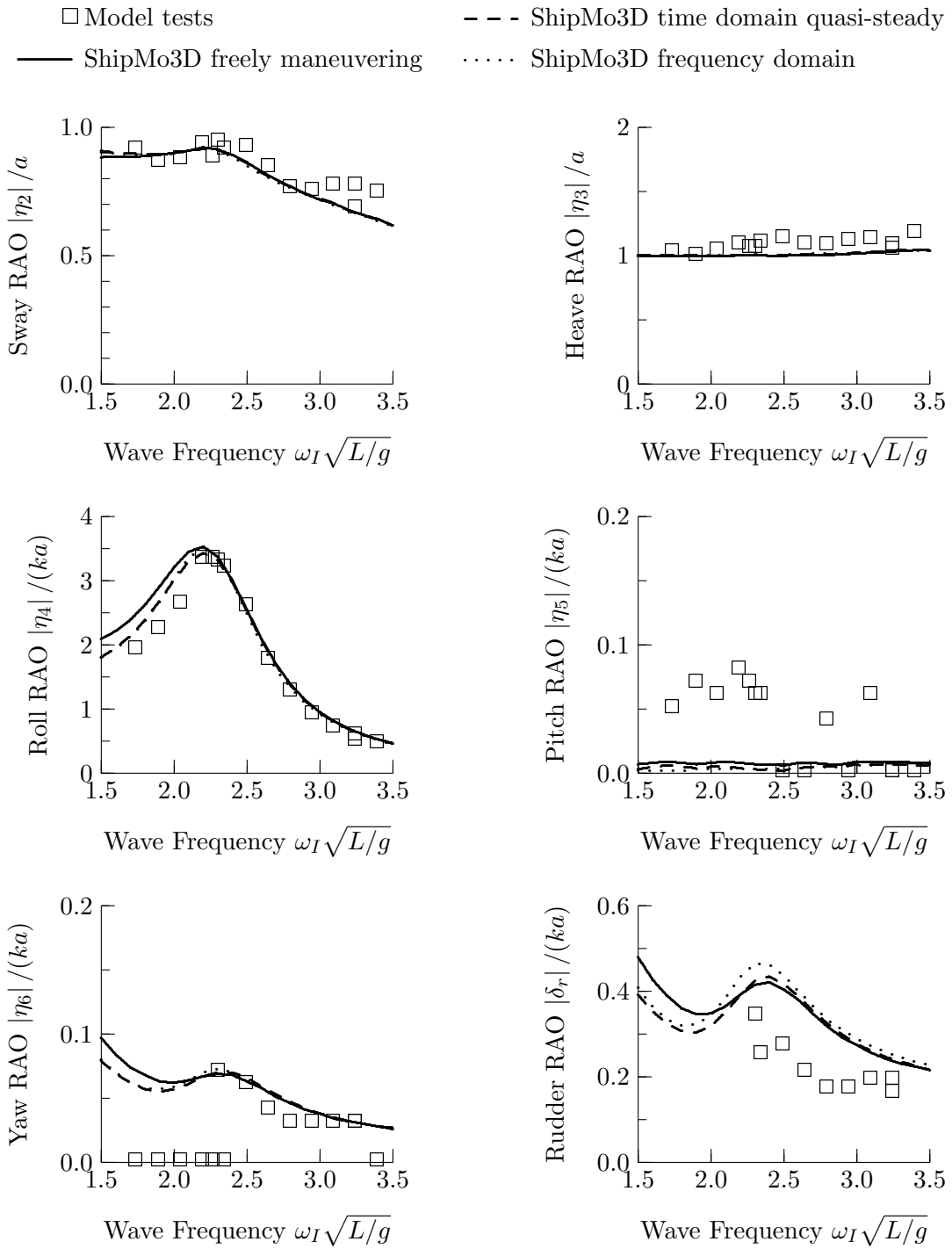

Figure 27: *RAOs for Steered Warship, Stern Quartering Seas at 90 degrees, Froude Number 0.18*

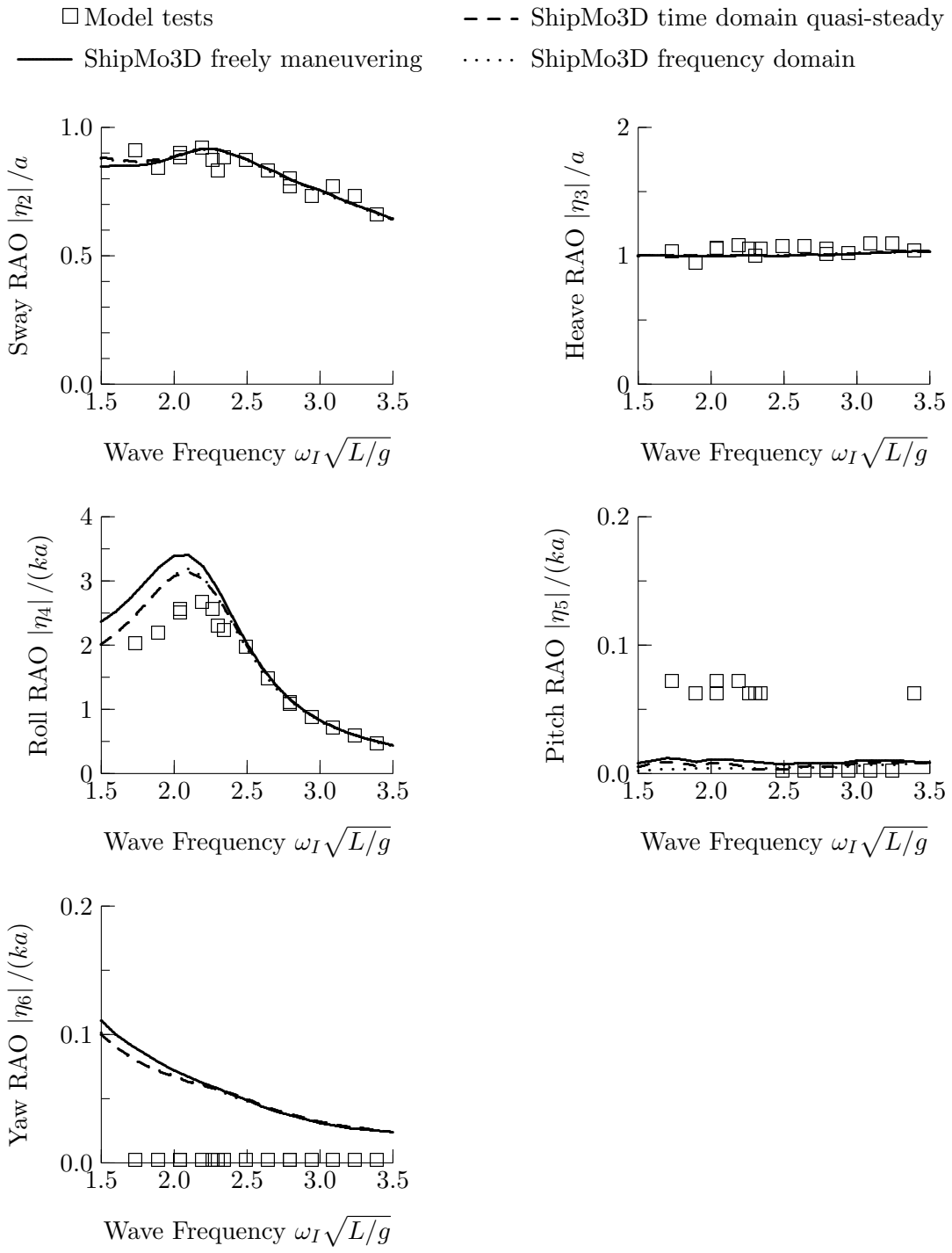

Figure 28: *RAOs for Steered Warship, Stern Quartering Seas at 90 degrees, Froude Number 0.28*

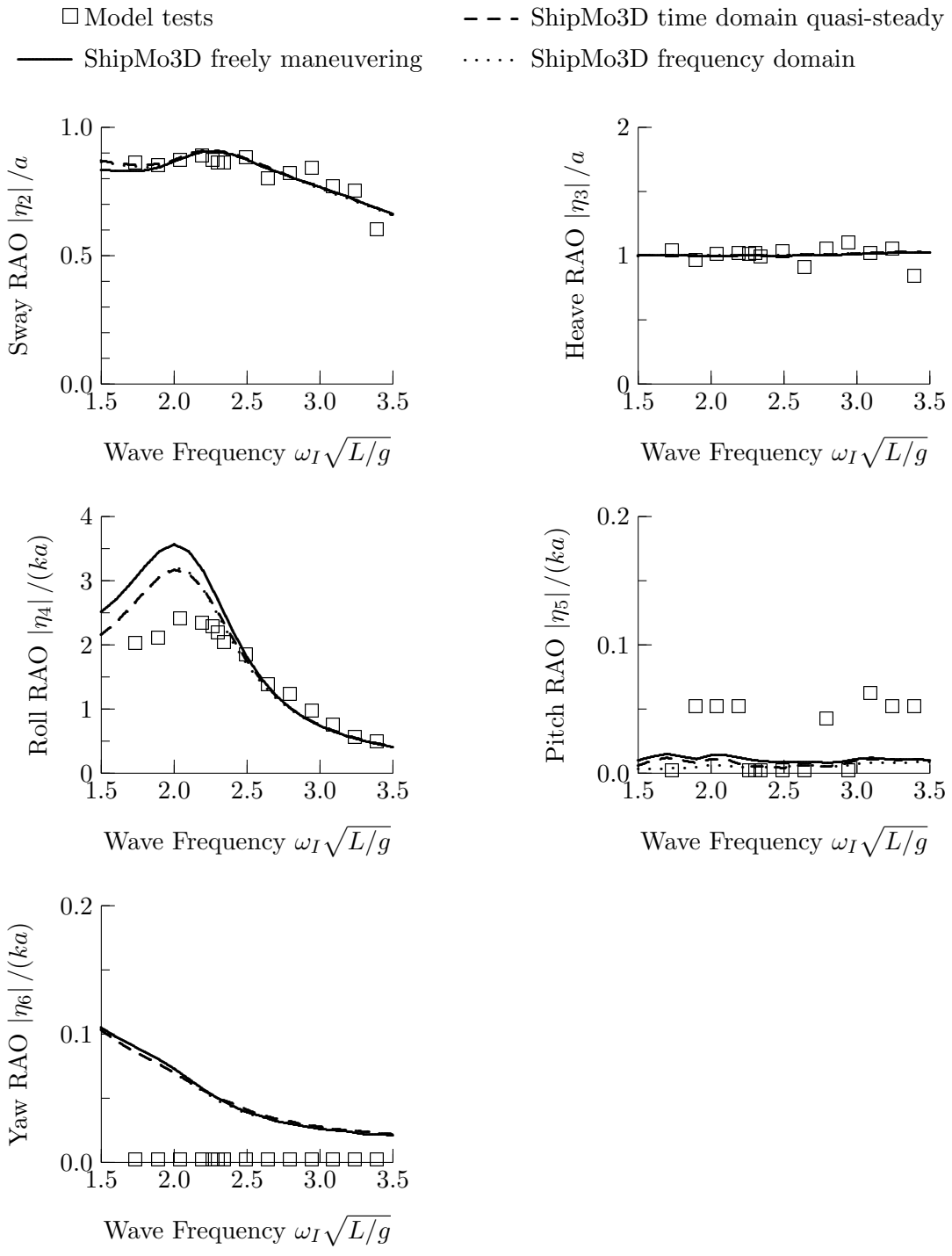

Figure 29: *RAOs for Steered Warship, Stern Quartering Seas at 90 degrees, Froude Number 0.36*

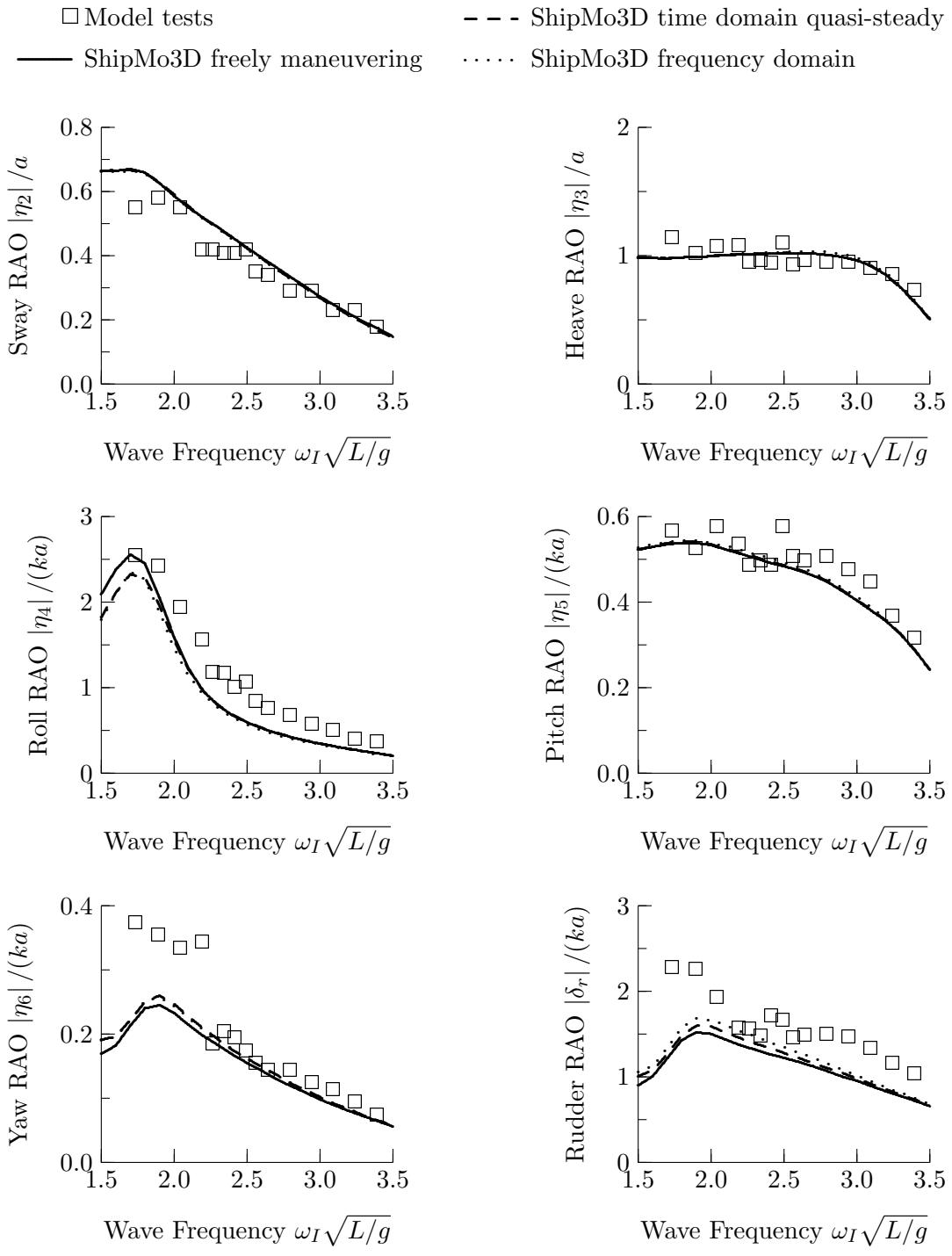

Figure 30: *RAOs for Steered Warship, Stern Quartering Seas at 120 degrees, Froude Number 0.27*

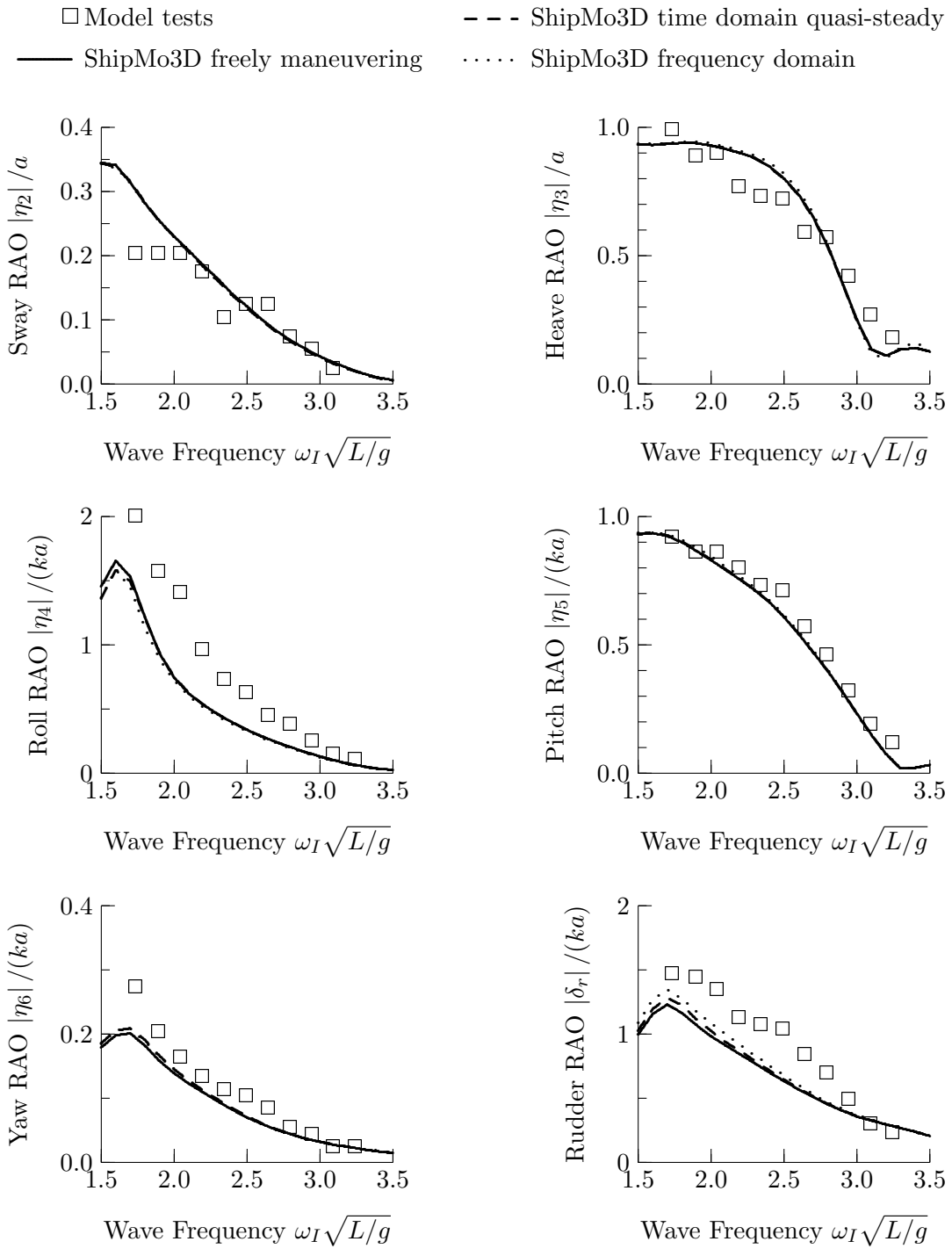

Figure 31: *RAOs for Steered Warship, Stern Quartering Seas at 150 degrees, Froude Number 0.26*

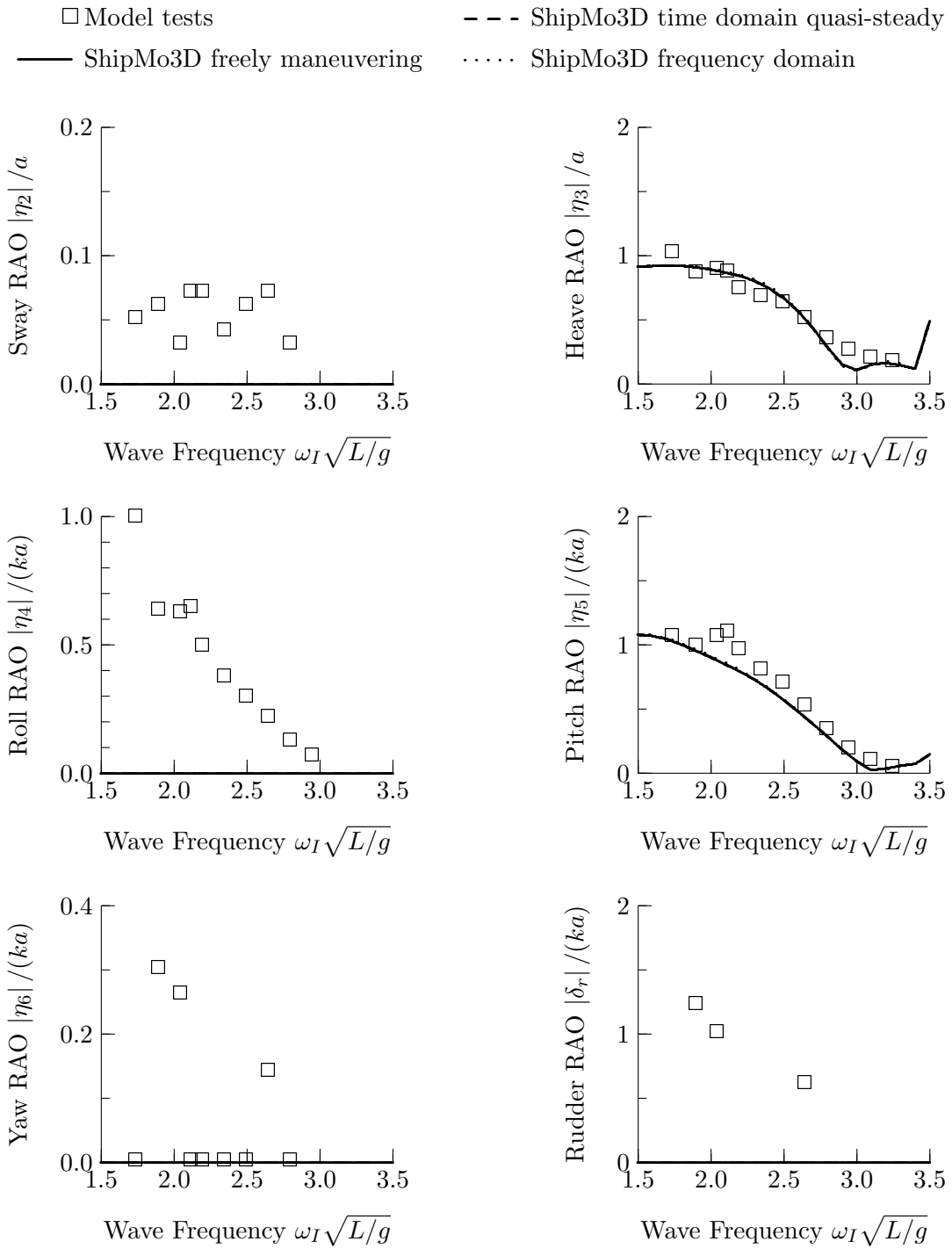

Figure 32: *RAOs for Steered Warship, Stern Quartering Seas at 180 degrees, Froude Number 0.26*

14 Recommendations

When computing the motions of a freely maneuvering ship, the greatest uncertainties in forces and resulting motions are due to hull maneuvering forces. In the field of maneuvering prediction, it is common practice to determine hull maneuvering force coefficients using model tests. It is recommended that future work examine methods for predicting hull maneuvering force coefficients. Computational fluid dynamics (CFD) is likely a very suitable approach for estimating hull maneuvering coefficients. Although CFD is likely too computationally intensive for direct simulation of ship maneuvering, prediction of maneuvering coefficients using CFD is likely feasible.

Regression methods for predicting hull maneuvering coefficients, such as those presented in Section 4, are much easier to apply than CFD predictions. The equations developed by Inoue et al. [10] are based on data for commercial ships. Regression equations based on data for naval hull forms could be very useful. It is also recommended that regression approaches be developed that account for the difference in profiles between various ship types. For example, the shallow draft at the stern of modern naval frigates likely causes hull maneuvering force coefficients to be significantly different from those ships with constant draft in the aft portion.

15 Conclusions

The ShipMo3D library has been extended to model freely maneuvering ships in calm water and in waves. New force components have been added, including hull maneuvering, hull resistance, propulsion, and rudder-propeller interaction. Comparisons of turning circle predictions with full-scale trials data for the tanker Esso Osaka give encouraging results. Comparisons of predictions with motions of a steered warship model in waves give very good results. Excellent agreement between predictions for a freely maneuvering ship and for a ship with quasi-steady speed and heading indicates that the extension of ShipMo3D to freely maneuvering ships has been correctly implemented. It is recommended that future work further investigate prediction of hull maneuvering forces.

References

[1] McTaggart, K.A. (2002). Three Dimensional Ship Hydrodynamic Coefficients Using the Zero Forward Speed Green Function. (DRDC Atlantic TM 2002-059). Defence Research and Development Canada - Atlantic.

[2] McTaggart, K.A. (2003). Hydrodynamic Forces and Motions in the Time Domain for an Unappended Ship Hull. (DRDC Atlantic TM 2003-104). Defence Research and Development Canada - Atlantic.

[3] McTaggart, K.A. (2003). Modelling and Simulation of Seaways in Deep Water for Simulation of Ship Motions. (DRDC Atlantic TM 2003-190). Defence Research and Development Canada - Atlantic.

[4] McTaggart, K.A. (2004). Appendage and Viscous Forces for Ship Motions in Waves. (DRDC Atlantic TM 2004-227). Defence Research and Development Canada - Atlantic.

[5] Bertram, V. (2000). Practical Ship Hydrodynamics, Oxford: Butterworth-Heinemann.

[6] (2002). The Specialist Committee on Esso Osaka - Final Recommendations to the 23rd ITTC. In *23rd International Towing Tank Conference*, Vol. II, pp. 573–609. The Hague.

[7] Barr, R. (1993). A Review and Comparison of Ship Maneuvering Simulation Methods. *Transactions, Society of Naval Architects and Marine Engineers*, **101**, 609–635.

[8] Burcher, R.K. (1991). The Prediction of the Manoeuvring Characteristics of Vessels. In *The Dynamics of Ships*, London: The Royal Society.

[9] Crane, C.L., Eda, H., and Landsburg, A. (1989). Principles of Naval Architecture, Volume III, Ch. 9, Controllability. Society of Naval Architects and Marine Engineers.

[10] Inoue, S., Hirano, M., and Kijima, K. (1981). Hydrodynamic Derivatives on Ship Manoeuvring. *International Shipbuilding Progress*, **28**(321), 112–125.

[11] Newman, J.N. (1977). Marine Hydrodynamics, Cambridge, Massachusetts: MIT Press.

[12] van Manen, J.D. and van Oossanen, P. (1988). Principles of Naval Architecture, Volume II, Ch. 5, Resistance. Society of Naval Architects and Marine Engineers.

[13] Holtrop, J. and Mennen, G.G.J. (1978). A Statistical Power Prediction Method. *International Shipbuilding Progress*, **25**(290), 253–256.

[14] Holtrop, J. and Mennen, G.G.J. (1982). An Approximate Power Prediction Method. *International Shipbuilding Progress*, **29**(335), 166–170.

[15] Holtrop, J. (1984). A Statistical Re-analysis of Resistance and Propuslion Data. *International Shipbuilding Progress*, **31**(363), 272–276.

[16] van Manen, J.D. and van Oossanen, P. (1988). Principles of Naval Architecture, Volume II, Ch. 6, Propulsion. Society of Naval Architects and Marine Engineers.

[17] Inoue, S., Hirano, M., Kijima, K., and Takashina, J. (1981). A Practical Calculation Method of Ship Manoeuvring Motion. *International Shipbuilding Progress*, **28**(325), 207–222.

[18] Söding, H. (1998). Limits of Potential Theory in Rudder Flow Predictions. In *22nd Symposium on Naval Hydrodynamics*, Washington.

[19] Smith, T.C. (1999). T-ADC(X) Maneuvering in Waves Study Using FREDYN. (Report NSWCCD-50-TR-1999\038). NSWCCD.

[20] Crane, C.L., Jr. (1979). Maneuvering Trials of the 278,000 DWT Esso Osaka in Shallow and Deep Water. *Transactions, Society of Naval Architects and Marine Engineers*, Vol. 87.

[21] Todd, F.H. (1953). Some Further Experiments on Single-Screw Merchant Ship Forms - Series 60. *Transactions, Society of Naval Architects and Marine Engineers*, **61**, 516–589.

[22] McTaggart, K., Datta, I., Stirling, A., Gibson, S., and Glen, I. (1997). Motions and Loads of a Hydroelastic Frigate Model in Severe Seas. *Transactions, Society of Naval Architects and Marine Engineers*, Vol. 105.

[23] Schmitke, R.T. and Murdey, D.C. (1980). Seakeeping and Resistance Trade-Offs in Frigate Hull Form Design. In *Thirteenth Symposium on Naval Hydrodynamics*, Tokyo.

[24] McTaggart, K. and Stredulinsky, D. (2004). Validation of Ship Motion Predictions with Sea Trials Data for a Naval Destroyer in Multidirectional Seas. In *25th Symposium on Naval Hydrodynamics*, St. Johns, Canada.

[25] Lloyd, A.R.J.M. and Crossland, P. (1990). Motions of a Steered Model Warship in Oblique Waves. *Transactions, Royal Institution of Naval Architects*, **132**, 79–98.

Symbols and Abbreviations

$[A]$	ship added mass matrix
$[A^{bk-i}]$	added mass matrix for bilge keel i
$[A^{foil-i}]$	added mass matrix for static foil i
$[A^{hull}]$	hull added mass matrix
$\partial \widetilde{A^{hull}}_{jk}/\partial x$	hull added mass x-derivative term
A_k	area of hull panel k
$[A^{rudder-i}]$	added mass matrix for rudder i
$[A^{skeg-i}]$	added mass matrix for skeg i
A_y	hull lateral profile area
A_{y-i}	lateral profile area of section i
A_w	hull wetted surface area
a	wave amplitude
B	beam
$[B]$	ship damping matrix
$[B^{bk-i}]$	damping matrix for bilge keel i
$[B^{foil-i}]$	damping matrix for static foil i
$[B^{hull-man}]$	hull maneuvering damping matrix
$B^{hull-man}_{ijU}$	hull maneuvering damping speed term
$B^{hull-man}_{ijU\|r'\|}$	hull maneuvering damping speed and yaw velocity term
$B^{hull-man}_{ijUr'^2}$	hull maneuvering damping speed and yaw velocity squared term
$B^{hull-man}_{ijU\|v'\|}$	hull maneuvering damping speed and drift velocity term
$B^{hull-man}_{ijUv'^2}$	hull maneuvering damping speed and drift velocity squared term
$B^{hull-rad}_{ijU}$	hull radiation damping speed term
$[B^{hull-visc}]$	hull viscous damping matrix due to roll
$[B^{rudder-i}]$	damping matrix for rudder i
$[B^{skeg-i}]$	damping matrix for skeg i
$[b^{hull-rad}]$	hull frequency independent damping matrix due to the potential flow
$[C]$	ship stiffness matrix
C_B	block coefficient
$[C^{bk-i}]$	lift stiffness matrix for bilge keel i
$[C^{buoy}]$	hull buoyancy stiffness matrix
C_{Dx}	hull resistance coefficient

C_{Dy}	hull cross-flow drag coefficient
$[C^{foil-i}]$	lift stiffness matrix for static foil i
$[C^{hull-man}]$	hull stiffness matrix due to maneuvering forces
$[C^{rudder-i}]$	lift stiffness matrix for rudder i
$[C^{rudder}_{i\delta}]$	rudder force stiffness due to rudder deflection
$C^{rudder-prop}$	rudder-propeller interaction coefficient
$[C^{skeg-i}]$	lift stiffness matrix for skeg i
C_{th}	propeller thrust loading coefficient
$\overline{c}$	mean chord length
$[c^{hull}]$	hull frequency independent stiffness matrix due to potential flow
c_{rudder}	rudder chord length
D_{prop}	propeller diameter
F_j	force component j in translating earth axes
$\{F^{cross}\}$	cross-flow drag vector
$\{F^D\}$	diffracted wave excitation force vector
$\{F^I\}$	incident wave excitation force vector
$\{F^{I-bk-i}\}$	incident wave force vector on bilge keel i
$\{F^{I-foil-i}\}$	incident wave force vector on foil i
$\{F^{I-hull}\}$	incident wave force vector on the hull
$\{F^{I-rudder-i}\}$	incident wave force vector on rudder i
$\{F^{I-skeg-i}\}$	incident wave force vector on skeg i
$\{F^{prop}\}$	propulsion force vector
$\{F^{resist}\}$	resistance force vector
$\{F^{rudder}_N\}$	normal force on rudder
$\{F^{rudder-deflect}\}$	rudder force vector due to rudder deflection
$F^{rudder-prop}_{drag}$	rudder-propeller interaction drag force
$F^{rudder-prop}_{lift}$	rudder-propeller interaction lift force
$F^{rudder-prop-ij}$	interaction force on rudder i from propeller j
$\{F^S\}$	force vector in ship-based axes
g	gravitational acceleration
J_T	propeller advance coefficient
$[K^{hull}]$	hull retardation damping matrix
K_T	propeller thrust coefficient
$\overline{KG}$	vertical centre of gravity relative to baseline

k	wave number
$k(i,j)$	global hull panel index for panel j on longitudinal segment i
$k^a_{\delta j}$	rudder acceleration gain for motion mode j
$k^d_{\delta j}$	rudder displacement gain for motion mode j
$k^v_{\delta j}$	rudder velocity gain for motion mode j
L	ship length between perpendiculars
l_β	term used for evaluating yaw-sway maneuvering coefficient
$[M]$	ship inertia matrix
N_{p-i}	number of hull panels with centroid lying within hull longitudinal segment i
N'_r	linear yaw-yaw maneuvering force coefficient
$N'_{r\|r\|}$	yaw velocity dependent nonlinear yaw-yaw maneuvering force coefficient
N'_{rv^2}	sway velocity dependent nonlinear yaw-yaw maneuvering force coefficient
N_{seg}	number of hull longitudinal sections
N'_v	linear yaw-sway maneuvering force coefficient
N'_{vr^2}	yaw velocity dependent nonlinear yaw-sway maneuvering force coefficient
n_{prop}	propeller speed in revolutions per second
n_{y-k}	y normal component for hull panel k
RPM^{prop}	propeller RPM
RPM^{prop}_C	command propeller RPM
r'	non-dimensional yaw velocity
r_{xx}	roll radius of gyration
r_{yy}	pitch radius of gyration
r_{zz}	yaw radius of gyration
s_{rudder}	rudder span
T	draft
T_{mid}	draft at midships
t	time
t_{prop}	propeller thrust deduction coefficient
t_{stern}	trim by stern
U	ship speed
v'	non-dimensional sway velocity
v^{cross}	cross-flow velocity

w_{prop}	propeller wake fraction
x, y, z	coordinates in translating earth axes
$\overline{x}_{Ay-i}$	nominal x coordinate of section i
x^f, y^f	horizontal plane coordinates in earth-fixed coordinate system
$\overline{x}_k$	x coordinate of the centroid of hull panel k
x^S, y^S, z^S	coordinates in ship-fixed axes
$\overline{x}^S, \overline{y}^S, \overline{z}^S$	location of rudder centroid in ship-based axes
Y'_r	linear sway-yaw maneuvering force coefficient
$Y'_{v\|r\|}$	yaw velocity dependent nonlinear sway-yaw maneuvering force coefficient
Y'_v	linear sway-sway maneuvering force coefficient
$Y'_{v\|r\|}$	yaw velocity dependent nonlinear sway-sway maneuvering force coefficient
$Y'_{v\|v\|}$	sway velocity dependent nonlinear sway-sway maneuvering force coefficient
$\overline{z}^{hull-man}$	effective vertical location of hull maneuvering forces
$\overline{z}_{Ay-i}$	nominal z coordinate of the underwater profile for hull longitudinal segment i
$\overline{z}_k$	z coordinate of the centroid of hull panel k
$\overline{z}_{wl}^{CG}$	z coordinate of ship centre of gravity relative to calm waterline
β	wave direction relative to ship
Γ_{rudder}	rudder dihedral angle (0°for rudder to port, 90°for rudder upward)
$\Delta\chi$	change in heading
δ^{rudder}	rudder deflection angle
δ_C^{rudder}	command rudder angle
δ_{max}^{rudder}	maximum rudder deflection
$\dot{\delta}_{max}^{rudder}$	maximum rudder velocity
ζ_{RPM}	propeller RPM response damping
ζ_δ	rudder nondimensional damping response constant
η_j	ship motion displacement for mode j in translating-earth coordinate system
η_j^f	ship motion displacement for mode j in earth-fixed coordinate system
$\dot{\eta}_j$	ship motion velocity for mode j in translating-earth coordinate system

η^f_{Cj}	command displacement for mode j in translating-earth coordinate system
ν	wave direction (from) in earth-fixed axes
ρ	water density
χ	ship heading (to) in earth-fixed axes
ω_e	encounter frequency
ω_I	incident wave frequency
ω_{RPM}	propeller RPM response natural frequency
ω_δ	rudder response natural frequency
$\triangle$	displacement

DOCUMENT CONTROL DATA

(Security classification of title, abstract and indexing annotation must be entered when document is classified)

1. ORIGINATOR (the name and address of the organization preparing the document).
Defence R&D Canada - Atlantic

2. SECURITY CLASSIFICATION (overall security classification of the document including special warning terms if applicable)
UNCLASSIFIED

3. TITLE (The complete document title as indicated on the title page. Its classification should be indicated by the appropriate abbreviation (S,C,R or U) in parentheses after the title.)
Simulation of Hydrodynamic Forces and Motions for a Freely Maneuvering Ship in a Seaway

4. AUTHORS (Last name, first name, middle initial. If military, show rank, e.g. Doe, Maj. John E.)
McTaggart, Kevin A.

5. DATE OF PUBLICATION (month and year of publication of document)
December 2005

6a. NO. OF PAGES (total including Annexes, Appendices, etc).
70

6b. NO. OF REFS (total cited in document)
25

7. DESCRIPTIVE NOTES (The category of the document, e.g. technical report, technical note or memorandum. If appropriate, enter the type of report, e.g. interim, progress, summary, annual or final.)
Technical Memorandum

8. SPONSORING ACTIVITY (the name of the department project office or laboratory sponsoring the research and development. Include address).
Defence R&D Canada - Atlantic, PO Box 1012, Dartmouth, NS, Canada B2Y 3Z7

9a. PROJECT OR GRANT NO. (If appropriate, the applicable research and development project or grant number under which the document was written.)
11GK12

9b. CONTRACT NO. (if appropriate, the applicable number under which the document was written).

10a. ORIGINATOR'S DOCUMENT NUMBER (the official document number by which the document is identified by the originating activity. This number must be unique.)
DRDC Atlantic TM 2005-071

10b. OTHER DOCUMENT NOs. (Any other numbers which may be assigned this document either by the originator or by the sponsor.)

11. DOCUMENT AVAILABILITY (any limitations on further dissemination of the document, other than those imposed by security classification)

(X) Unlimited distribution
( ) Defence departments and defence contractors; further distribution only as approved
( ) Defence departments and Canadian defence contractors; further distribution only as approved
( ) Government departments and agencies; further distribution only as approved
( ) Defence departments; further distribution only as approved
( ) Other (please specify):

12. DOCUMENT ANNOUNCEMENT (any limitation to the bibliographic announcement of this document. This will normally correspond to the Document Availability (11). However, where further distribution (beyond the audience specified in (11) is possible, a wider announcement audience may be selected).

13. ABSTRACT (a brief and factual summary of the document. It may also appear elsewhere in the body of the document itself. It is highly desirable that the abstract of classified documents be unclassified. Each paragraph of the abstract shall begin with an indication of the security classification of the information in the paragraph (unless the document itself is unclassified) represented as (S), (C), (R), or (U). It is not necessary to include here abstracts in both official languages unless the text is bilingual).

ShipMo3D is DRDC Atlantic's object-oriented library for modelling of ship motions in waves. Previous ShipMo3D developed considered ships travelling with quasi-steady speed and heading. This report describes the extension of the ShipMo3D library to model motions of freely maneuvering ships. New ShipMo3D force components arise from hull maneuvering, resistance, propulsion, and rudder-propeller interaction. Comparisons of turning circle predictions with full-scale trials data for the tanker Esso Osaka give encouraging results. Comparisons of predictions with motions of a steered warship model in waves give very good results. Excellent agreement between predictions for a freely maneuvering ship and for a ship with quasi-steady speed and heading indicates that the extension of ShipMo3D to freely maneuvering ships has been correctly implemented. It is recommended that future work further investigate prediction of hull maneuvering forces.

14. KEYWORDS, DESCRIPTORS or IDENTIFIERS (technically meaningful terms or short phrases that characterize a document and could be helpful in cataloguing the document. They should be selected so that no security classification is required. Identifiers, such as equipment model designation, trade name, military project code name, geographic location may also be included. If possible keywords should be selected from a published thesaurus. e.g. Thesaurus of Engineering and Scientific Terms (TEST) and that thesaurus-identified. If it not possible to select indexing terms which are Unclassified, the classification of each should be indicated as with the title).

maneuvering
propulsion
resistance
roll
sway
seakeeping
ship motions
simulation
yaw

This page intentionally left blank.

Defence R&D Canada

Canada's leader in defence
and National Security
Science and Technology

R & D pour la défense Canada

Chef de file au Canada en matière
de science et de technologie pour
la défense et la sécurité nationale

www.drdc-rddc.gc.ca